Multimodal cartography of human lymphopoiesis reveals B and T/NK/ILC lineages are subjected to differential regulation

Kutaiba Alhaj Hussen, Emna Chabaane, Elisabeth Nelson, Shalva Lekiashvili, Samuel Diop, Seydou Keita, Bertrand Evrard, Aurélie Lardenois, Marc Delord, Els Verhoeyen, et al.

iScience

CellPress
OPEN ACCESS

Article

Multimodal cartography of human lymphopoiesis reveals B and T/NK/ILC lineages are subjected to differential regulation

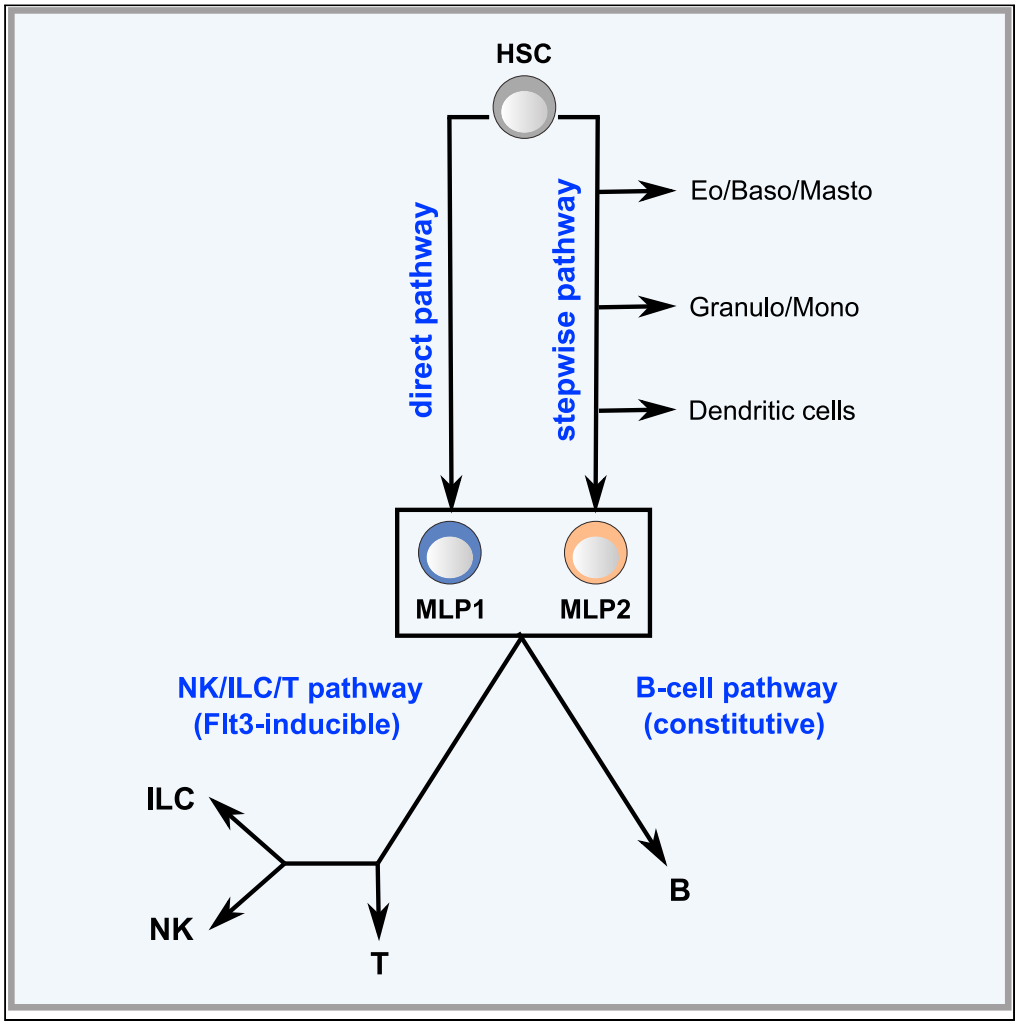

Kutaiba Alhaj Hussen, Emna Chabaane, Elisabeth Nelson, ..., Vahid Asnafi, Frederic Chalmel, Bruno Canque

bruno.canque@ephe.psl.eu

Highlights

Lymphoid specification follows direct or stepwise routes converging toward MLPs

MLPs undergo a proliferation arrest before entering NK/ILC/T or B lymphoid pathways

Differentiation along the NK/ILC/T pathway is inducible by Flt3 signaling

Differentiation along the B pathway is regulated cell-intrinsically

Alhaj Hussen et al., iScience 26, 107890
October 20, 2023
https://doi.org/10.1016/j.isci.2023.107890

iScience

CellPress
OPEN ACCESS

Article

Multimodal cartography of human lymphopoiesis reveals B and T/NK/ILC lineages are subjected to differential regulation

Kutaiba Alhaj Hussen,[1,2] Emna Chabaane,[1] Elisabeth Nelson,[1] Shalva Lekiashvili,[1] Samuel Diop,[1] Seydou Keita,[1] Bertrand Evrard,[3] Aurélie Lardenois,[3] Marc Delord,[1] Els Verhoeyen,[4,5] Kerstin Cornils,[6] Zeinab Kasraian,[1,7] Elizabeth A. Macintyre,[7] Ana Cumano,[8] David Garrick,[1] Michele Goodhardt,[1] Guillaume P. Andrieu,[7] Vahid Asnafi,[7] Frederic Chalmel,[3,9] and Bruno Canque[1,9,10,*]

SUMMARY

The developmental cartography of human lymphopoiesis remains incompletely understood. Here, we establish a multimodal map demonstrating that lymphoid specification follows independent direct or stepwise hierarchic routes converging toward the emergence of newly characterized CD117^{lo} multi-lymphoid progenitors (MLPs) that undergo a proliferation arrest before entering the CD127^{-} (NK/ILC/T) or CD127^{+} (B) lymphoid pathways. While the differentiation of CD127^{-} early lymphoid progenitors is mainly driven by Flt3 signaling, emergence of their CD127^{+} counterparts is regulated cell-intrinsically and depends exclusively on the divisional history of their upstream precursors, including hematopoietic stem cells. Further, transcriptional mapping of differentiation trajectories reveals that whereas myeloid granulomonocytic lineages follow continuous differentiation pathways, lymphoid trajectories are intrinsically discontinuous and characterized by sequential waves of cell proliferation allowing pre-commitment amplification of lymphoid progenitor pools. Besides identifying new lymphoid specification pathways and regulatory checkpoints, our results demonstrate that NK/ILC/T and B lineages are under fundamentally distinct modes of regulation. (149 words)

INTRODUCTION

Hematopoiesis is defined as the physiological process by which multipotent, lineage-specified stem/progenitor and precursor cells self-renew or differentiate along divergent pathways to ensure the lifelong production of platelets, red blood cells, and leukocytes. Over the last decade, single-cell genomics and fate mapping studies have revealed a previously unsuspected functional heterogeneity within the hematopoietic stem/progenitor cell (HSPC) compartment. Together these studies suggest that rather than as a stepwise hierarchy comprising distinct populations, hematopoiesis is organized as a developmental continuum where hematopoietic stem cells (HSCs) feed a continuous flux of differentiation along the different lineage branches.[1] As well as passing through intermediate stages of multipotent progenitors, it is now clear that HSCs can directly commit toward the erythroid or megakaryocytic lineages[2–4] or enter the granulocytic or monocytic lineages in response to myeloid growth factors.[5,6] Consistent with this, clonal scale *in vivo* tracking of HSC differentiation under steady-state or regenerative conditions in mouse[7,8] or non-human primate[9] models, as well as transplanted patients,[10,11] provided evidence that lineage priming can be initiated at the level of HSCs. Despite this, there is still debate regarding when and how progenitors execute fate decisions and if lineage choices are primarily conditioned by intrinsic cell properties, stochastic behavior or dictated by extracellular signals.[12] Further, increasing evidence indicates that lymphoid and myeloid lineages are subjected to distinct developmental constraints. This is supported by transplantation studies showing that the early emergence of myeloid cells contrasts with the delayed lymphoid reconstitution,[13,14] as

[1]INSERM U976, Université de Paris, École Pratique des Hautes Études/PSL Research University, Institut de Recherche Saint Louis, Paris, France
[2]Service de Biochimie, Université de Paris Saclay, Hôpital Paul Brousse, AP-HP, Villejuif, Paris, France
[3]University Rennes, Inserm, EHESP, Irset (Institut de recherche en santé, environnement et travail) - UMR_S 1085, F-35000 Rennes, France
[4]CIRI, International Center for Infectiology Research, Université de Lyon, INSERM U1111, Lyon, France
[5]Centre Mediterranéen de Médecine Moléculaire (C3M), INSERM U1065, Nice, France
[6]Division of Pediatric Stem Cell Transplantation and Immunology, Department of Pediatric Hematology and Oncology, University Medical Center Hamburg-Eppendorf and Research Institute Children's Cancer Center, Hamburg, Germany
[7]Institut Necker Enfants-Malades, INSERM U1151, Hôpital Necker Enfants-Malades, Laboratoire d'Onco-Hématologie, Assistance Publique-Hôpitaux de Paris (AP-HP), Université de Paris, Paris, France
[8]Unit of Lymphopoiesis, Immunology Department, Institut Pasteur, Paris, France
[9]These authors contributed equally
[10]Lead contact
*Correspondence: bruno.canque@ephe.psl.eu
https://doi.org/10.1016/j.isci.2023.107890

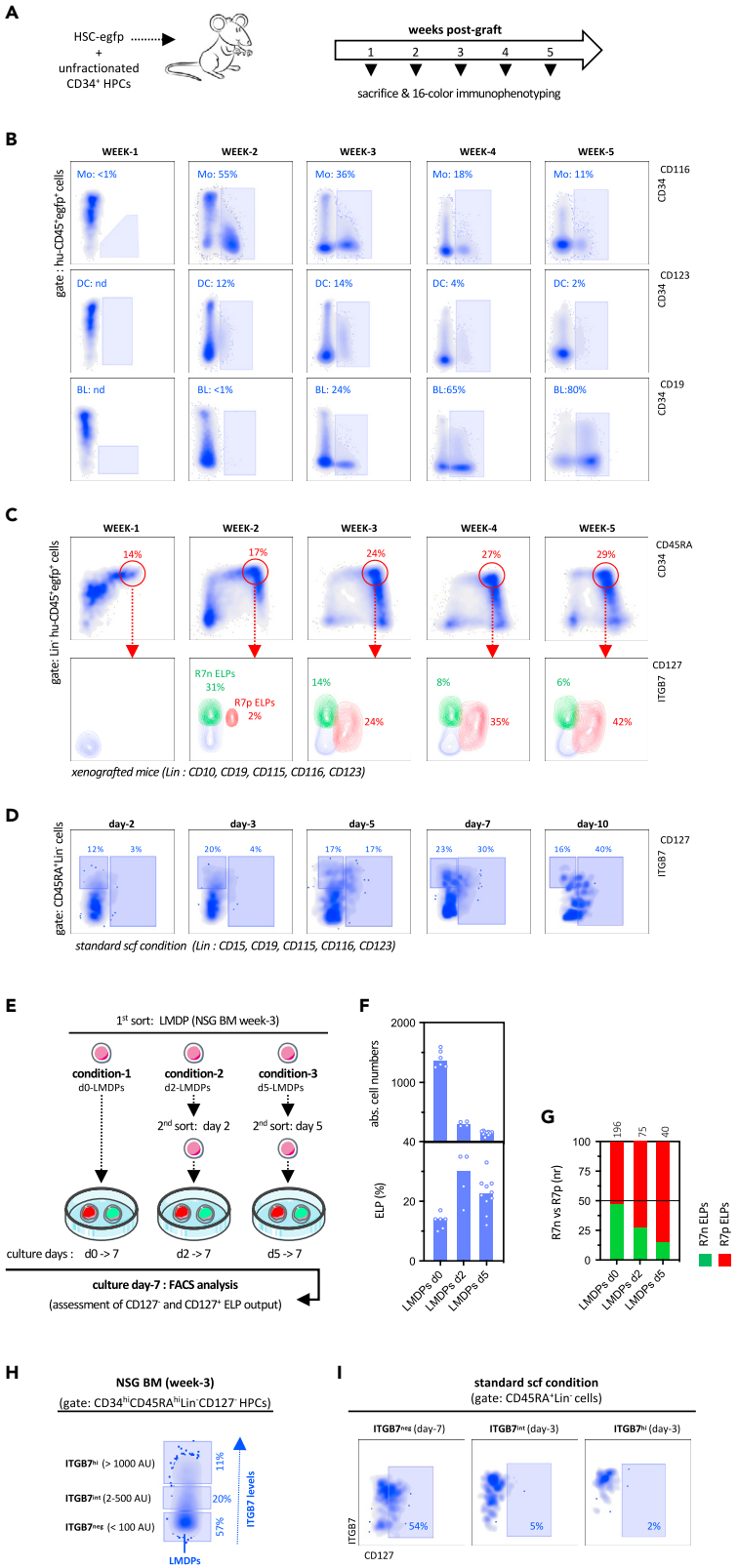
A
HSC-egfp
+
unfractionated
CD34+ HPCs
weeks post-graft
1
2
3
4
5
sacrifice & 16-color immunophenotyping
B
WEEK-1
WEEK-2
WEEK-3
WEEK-4
WEEK-5
gate : hu-CD45+egfp+ cells
Mo: <1%
Mo: 55%
Mo: 36%
Mo: 18%
Mo: 11%
CD116
CD34
DC: nd
DC: 12%
DC: 14%
DC: 4%
DC: 2%
CD123
CD34
BL: nd
BL: <1%
BL: 24%
BL:65%
BL:80%
CD19
CD34
C
WEEK-1
WEEK-2
WEEK-3
WEEK-4
WEEK-5
gate: Lin- hu-CD45+egfp+ cells
14%
17%
24%
27%
29%
CD45RA
CD34
R7n ELPs
31%
R7p ELPs
2%
14%
24%
8%
35%
6%
42%
CD127
ITGB7
xenografted mice (Lin : CD10, CD19, CD115, CD116, CD123)
D
day-2
day-3
day-5
day-7
day-10
gate: CD45RA+Lin- cells
12%
3%
20%
4%
17%
17%
23%
30%
16%
40%
CD127
ITGB7
standard scf condition (Lin : CD15, CD19, CD115, CD116, CD123)
E
1st sort: LMDP (NSG BM week-3)
condition-1
d0-LMDPs
condition-2
d2-LMDPs
condition-3
d5-LMDPs
2nd sort: day 2
2nd sort: day 5
culture days :
d0 -> 7
d2 -> 7
d5 -> 7
culture day-7 : FACS analysis
(assessment of CD127- and CD127+ ELP output)
F
abs. cell numbers
2000
1000
40
ELP (%)
20
0
LMDPs d0
LMDPs d2
LMDPs d5
G
R7n vs R7p (nr)
100
75
50
25
0
196
75
40
LMDPs d0
LMDPs d2
LMDPs d5
R7n ELPs
R7p ELPs
H
NSG BM (week-3)
(gate: CD34hiCD45RAhiLin-CD127- HPCs)
ITGB7hi (> 1000 AU)
ITGB7int (2-500 AU)
ITGB7neg (< 100 AU)
11%
20%
57%
ITGB7 levels
LMDPs
I
standard scf condition
(gate: CD45RA+Lin- cells)
ITGB7neg (day-7)
ITGB7int (day-3)
ITGB7hi (day-3)
54%
5%
2%
ITGB7
CD127

Figure 1. Dynamics of CD127$^-$ and CD127$^+$ ELPs in the BM of HSC-engrafted mice

(A) Experimental design: neonatal CD34^{hi}CD45RA$^-$CD38$^{lo/-}$Lin$^-$ progenitors (Lin: CD3, CD4, CD10, CD19, CD24, CD56, CD115, CD116, CD123, CD127, ITGB7; thereafter referred to as HSCs) pooled from different donors were transduced with *egfp*-reporter lentiviruses (1.5 × 10^5 cells/mouse) before mixing with non-transduced bulk CD34$^+$ HSPCs (1.5 × 10^5 cells/mouse) and intravenous injection to irradiated NSG mice. Note that non-transduced bulk CD34$^+$ HSPCs were used as carriers to ensure full comparability with mice reconstituted with LMDPs (see also Figures S1E and S1F). To follow multi-lineage reconstitution, hu-CD45$^+$egfp$^+$ cells harvested from the BM of mice sacrificed at weekly endpoints were analyzed by multiparameter flow cytometry; percentages of corresponding cell subsets are indicated; results from individual mice are representative of 3 independent experiments.

(B) Density plots showing the kinetics of monocytes (Mo; CD116$^+$CD123$^-$) (upper panels; blue rectangles), dendritic cells (DC; CD116$^+$CD123$^+$ (medium panels; blue rectangles) and B lymphocytes (BL CD19$^+$) (lower panels; blue rectangles) in the BM of xenografted mice.

(C) Asynchronous *in vivo* emergence of CD127$^-$ and CD127$^+$ ELPs. Upper density plots show the kinetics of CD34^{hi}CD45RA^{hi}Lin$^-$ HSPCs (red circles) in xenografted mice; gates are set on Lin$^-$ negative cells (Lin: CD115, CD116, CD123, CD10, CD19). Lower contour plots show the dynamics of CD127$^-$ (green) and CD127$^+$ (red) ELPs; blue lines correspond to LMDPs; red arrows show the gating strategy.

(D) Asynchronous *in vitro* emergence of CD127$^-$ and CD127$^+$ ELPs. LMDPs cultured under standard *scf* condition were analyzed by flow cytometry at the indicated time points; gates are set on CD45RA$^+$My$^-$CD19$^-$ cells (My$^-$: CD15$^-$, CD115$^-$, CD116$^-$, CD123$^-$; see also Figure S1C). Bidimensional density plots show the kinetics of differentiation of CD127$^-$ and CD127$^+$ ELPs. Data are from ≥ 10 concatenated wells; percentages of the corresponding populations are indicated. Results are from 1 representative experiment.

(E–G) Time-dependent changes in the lymphoid potential of cultured LMDPs. (E) Experimental design: LMDPs sorted from NSG mice at week-3 post-grafting were cultured by 100 cell-pools for 7 days onto OP9 stromal cells before analysis by flow cytometry (see also Figure S1C for the gating procedure). Condition-1 (d0-LMDPs; *left panel*): LMDPs are cultured for 7-day under the standard *scf* condition. Condition-2 (d2-LMDPs; *medium panel*): LMDPs sorted from cultures at day-2 are seeded for 5 more days in secondary cultures under the standard *scf* condition; Condition-3 (d5-LMDPs; *right panel*): LMDPs sorted from cultures at day-5 are seeded for 2 more days in secondary cultures under the standard *scf* condition. (F) Shown are absolute cell yields (upper panel) and median percentages of ELPs (lower panel); circles correspond to individual wells. (G) Stacked bar plot shows normalized ratios of CD127$^-$ (green) vs. CD127$^+$ (red) ELPs; median numbers of ELPs per well are indicated (upper row); positivity threshold for ELP detection is set arbitrarily at ≥ 10 ELPs/well. Results are expressed as medians of 4–9 replicates from a representative experiment.

(H and I) CD127$^-$ and CD127$^+$ ELPs emerge independently from LMDPs. (H) Density plot shows the gating strategy used for fractionation of CD34^{hi}CD45RA^{hi}CD127$^-$Lin$^-$ HPCs (Lin: CD10, CD19, CD115, CD116, CD123) from HSC-xenografted mice (week-3). (I) The indicated ITGB7$^{neg;\ int;\ hi}$ cellular fractions were sorted from the BM of mice at week-3 after grafting and then cultured for 3 or 7 days under the under standard *scf* condition before analysis by flow cytometry. Density plots show the percentages of in vitro-generated CD127$^+$ ELPs (blue rectangles); gates are set as aforementioned; results from one representative experiment are pooled from 10 concatenated wells. ITGB7^{neg} cells correspond to LMDPs.

well as by previous reports in the mouse that lymphoid specification initiates downstream of HSCs, at the level of lymphoid-primed multipotent progenitors (LMPPs).[15] LMPPs critically depend on Flt3 signaling for survival and expansion[16] and stepwise progression to downstream RAG1- or DNTT-expressing early or lymphoid-primed progenitors (ELPs/LPPs),[17–19] and then to IL7R/CD127$^+$ common lymphoid progenitors (CLPs).[20] Despite significant progresses over the past years, so far it remains unclear whether lymphoid differentiation pathways and gene regulatory networks have been conserved from mice to humans. Earlier human studies have provided evidence that upregulation of CD45RA by CD34^{hi} hematopoietic stem/progenitor cells (HSPCs) marks the loss of erythro-megakaryocytic potential[21,22] and that lymphoid fate co-segregates with granulomonocytic and dendritic potentials within the CD45RA$^+$ compartment.[23–25] Further fractionation of CD45RA$^+$ hematopoietic progenitors cells (HPCs) from the umbilical cord blood (UCB) led to identification of CD7[25,26] or CD10[23,27,28] multi-lymphoid progenitors (MLPs) whose functions and developmental statuses have long remained controversial.[29] Our recent demonstration that these populations correspond to embryonic (CD7$^+$), fetal (CD7$^-$) or postnatal (CD10$^+$) MLPs has revealed a previously unsuspected complexity of the developmental biology of the lymphoid lineage.[30]

To overcome constraints inherent to human studies due to donor effect, ontogeny-related changes in lymphoid architecture and bypass the limitations of studies based on the analysis of total BM cells[31,32] or bulk CD34$^+$ HSPCs[33,34] from primary fetal or postnatal donors which, due to the sparsity of lymphoid progenitors, do not allow optimal delineation of lymphoid differentiation trajectories, we have developed an *in-vivo* modeling approach of mid-fetal hematopoiesis in humanized mice.[35] This already led to the demonstration that human lymphopoiesis displays a bipartite organization stemming from founder populations of CD127$^-$ and CD127$^+$ ELPs and that, whereas the CD127$^-$ ELPs are mainly NK/ILC/T precursors, their CD127$^+$ counterparts are intrinsically biased toward the B lineage.[36] However, at present the precise origin of these ELPs, and the regulation of their developmental relationships are still unknown. In the current study, combining genetic barcoding with time course and endpoint molecular and functional analyses, we establish a multimodal roadmap for human lymphopoiesis. Our results demonstrate that CD127$^-$ and CD127$^+$ ELPs originate from canonical CD117^{lo} MLPs and that they are subject to divergent Flt3L-inducible versus cell-intrinsic regulatory mechanisms. Further, we show that CD117^{lo} MLPs arise from independent direct or stepwise differentiation pathways and provide evidence that lymphoid differentiation trajectories are intrinsically discontinuous and characterized by alternating phases of proliferation and differentiation.

As well as shedding a new light on human lymphopoiesis, the findings reported here may have important implications for our understanding of the origin and pathogenesis of primary immune deficiencies and acute lymphoblastic leukemia.

RESULTS

CD127$^-$ and CD127$^+$ ELP production patterns depend on the divisional history of their precursors

To get insight into the development relationships between CD127$^-$ and CD127$^+$ ELPs, we analyzed hematopoietic reconstitution in mice xenografted with neonatal CD45RA$^-$Lin$^-$ HSCs transduced with *egfp*-reporter lentiviruses (Figure 1A). Consistent with an earlier report,[14] dynamic

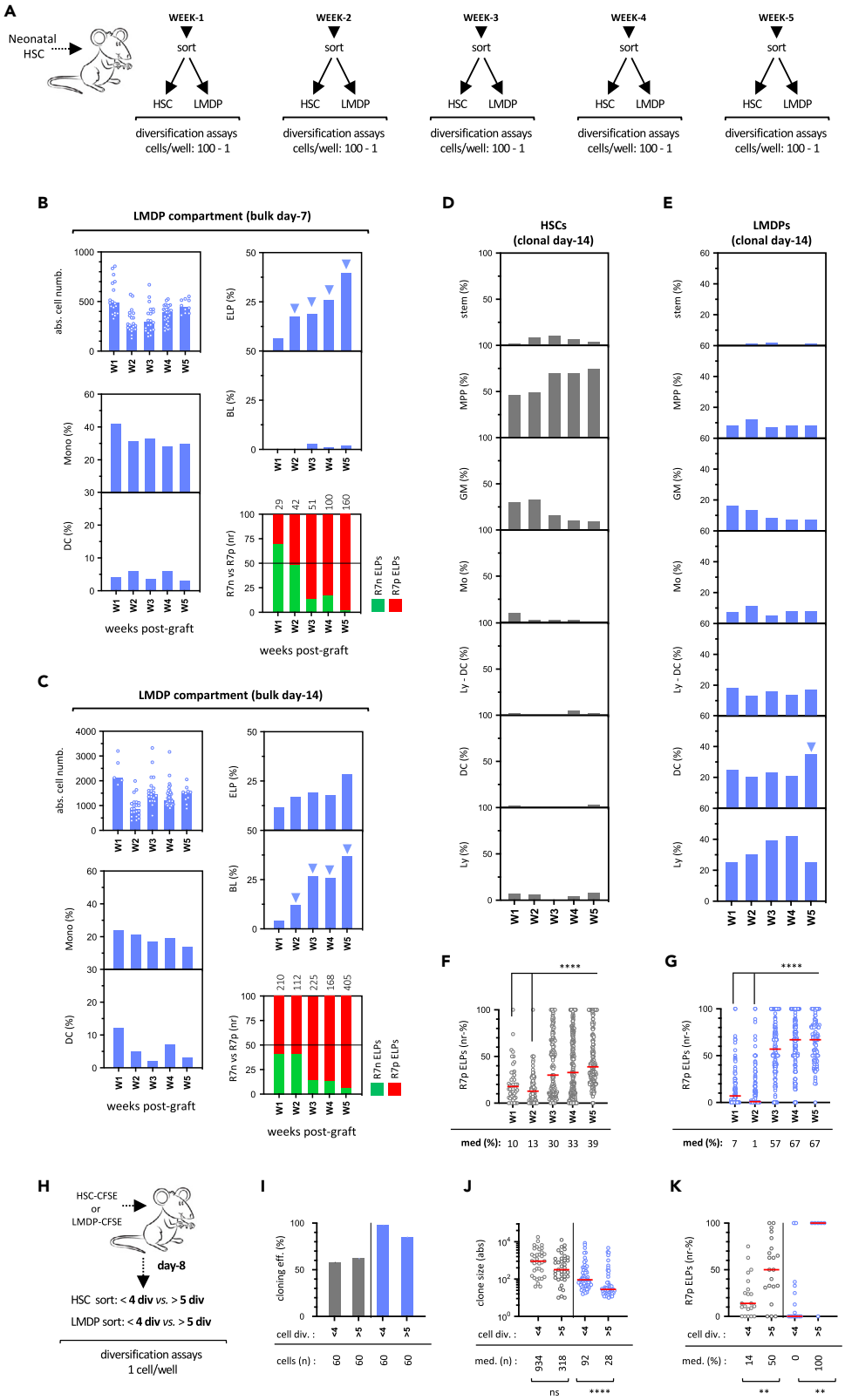
A
Neonatal HSC
WEEK-1
WEEK-2
WEEK-3
WEEK-4
WEEK-5
sort
HSC
LMDP
diversification assays
cells/well: 100 - 1
B
LMDP compartment (bulk day-7)
abs. cell numb.
ELP (%)
BL (%)
Mono (%)
DC (%)
R7n vs R7p (nr)
R7n ELPs
R7p ELPs
weeks post-graft
C
LMDP compartment (bulk day-14)
D
HSCs
(clonal day-14)
stem (%)
MPP (%)
GM (%)
Mo (%)
Ly - DC (%)
Ly (%)
E
LMDPs
(clonal day-14)
F
R7p ELPs (nr-%)
med (%): 10 13 30 33 39
G
med (%): 7 1 57 67 67
H
HSC-CFSE
or
LMDP-CFSE
day-8
HSC sort: < 4 div vs. > 5 div
LMDP sort: < 4 div vs. > 5 div
diversification assays
1 cell/well
I
cloning eff. (%)
cell div. :
cells (n) :
J
clone size (abs)
med. (n) :
ns
****
K
med. (%) :
**

Figure 2. *In vitro* assessment of lymphoid potential in multi-lineage diversification assays

(A) Experimental design: mice xenografted with neonatal HSCs were sacrificed at the indicated endpoints before assessment of HSC or LMDP lympho-myeloid potential in bulk or single-cell *in vitro* diversification assays.

(B and C) Assessment of lineage output in bulk diversification assays. LMDPs were cultured by 100 cell-pools for (B) 7 or (C) 14 days under standard *scf* condition before quantification of absolute cell yields and lineage outputs. Upper left panel: absolute cell yields (bars indicate median cell numbers; circles correspond to individual wells); lower left panels: median percentages of $CD115^+$ monocytes (top) and $CD123^+$ DC (bottom); upper right panels: median percentages of $CD127^{-/+}$ ELPs (top) and BLs (bottom); results are normalized relative to total hu-$CD45^+$ cells; lower right stacked bar plot showing normalized ratios of $CD127^-$ (green) vs. $CD127^+$ (red) ELPs; results expressed as median percentages of 5–20 replicates are from one representative experiment; median numbers of ELPs per well are indicated (upper row). Purple arrows show the time-dependent increase in ELP or B-cell outputs.

(D–G) Assessment of lineage output in clonal diversification assays. HSC or LMDPs were cultured for 14 days under *scf:gm-csf:tpo* condition before quantification of absolute cell yields and lineage outputs; positivity threshold for clone detection was set arbitrarily at $\geq$ 20 cells/clone.

(D and E) Bar plots show the dynamics of stem (Stem: $CD34^+$ cells $\geq$ 50%; others < 10%), multipotent (MPP: Gr $\geq$ 10%; Mono $\geq$ 10%; DC $\geq$ 10%; Ly $\geq$ 10%), granulomonocytic (GM: Gr + Mono $\geq$ 50%; others < 10%), monocytic (M: Mono $\geq$ 50%; others < 10%), lympho-dendritic (Ly-DC: Ly + DC $\geq$ 50%; others < 10%), dendritic (DC: $\geq$ 50%; others < 10%) or lymphoid (Ly: Ly: $\geq$ 50%; others < 10%) clones across the (D) HSC (gray bars) or (E) LMDP (blue bars) compartments; purple arrow shows the increase in DC progenitors observed at week-5 after grafting.

(F and G) Circle plots show the kinetics of $CD127^+$ ELPs within lymphoid-containing (F) HSC- or (G) LMDP-derived clones; results are normalized relative to total ELP content and expressed on a per clone basis. Red bars indicate medians; corresponding values are indicated (lower row); positivity threshold for ELP detection is set arbitrarily at $\geq$ 10 ELPs/clone). Assessment of statistical significance was performed with the Mann-Whitney test (****p < 0.0001; ***p < 0.001; **p < 0.01). Results are pooled from 2 experiments.

(H–K) Effect of conservative cell divisions on the lymphoid potential of HSC or LMDPs. (H) Experimental design: neonatal HSCs or LMDP were labeled with proliferation-dependent dye carboxyfluorescein diacetate succinimidyl ester (CFSE) prior to injection to irradiated NSG mice (2.5×10^5 cells/mouse). At day 8 after grafting, self-renewed HSCs or LMDPs subdivided according to the number of conservative cell divisions (< 4 versus > 5 divisions) were seeded by FACS in single-cell diversification assays. (I) Cloning efficiencies of divided (> 5) versus non-divided (< 4) HSCs (gray bars) or LMDPs (blue bars). (J) Absolute cell numbers per clone derived from divided versus non-divided HSCs (gray circles) or LMDPs (blue circles). (K) Relative percentages of $CD127^+$ ELPs detected among lymphoid-containing clones derived from divided versus non-divided HSCs (gray circles) or LMDPs (blue circles). Red bars indicate medians; corresponding values are indicated (lower row). Assessment of statistical significance was performed as aforementioned.

follow-up of recipient mice found that reconstitution of myeloid monocytic or dendritic lineages precedes that of B lymphocytes and disclosed a sequential emergence of $CD127^-$ and $CD127^+$ ELPs (Figures 1B and 1C; see also Figures S1A and S1B; Table S1). As expected, expansion of the B cell compartment closely paralleled with the increase in the production of $CD127^+$ ELPs. Overall similar, albeit accelerated, biphasic reconstitution patterns were observed in mice reconstituted with downstream $CD45RA^{hi}Lin^-$ LMDPs (lympho-myelo-dendritic progenitors)[36] that supported only transient hematopoietic reconstitution (Figures S2A and S2B). Subsequent analyses confirmed that beyond week-2 after grafting, percentages of $CD127^{-/+}$ ELP detected in HSC-engrafted mice closely match those observed in the BM of primary fetal or pediatric donors (Figures S1C–S1H).

To investigate whether sequential emergence of $CD127^-$ then $CD127^+$ ELPs reflects a temporal shift in the lymphoid potential, we then developed an *in vitro* diversification assay in which myeloid granulocyte (Gr; $CD15^+$), monocyte (Mo; $CD115^+$), and dendritic (DC; $CD123^+$) precursors, as well as lymphoid $CD127^-$ or $CD127^+$ ELPs and $CD19^+$ B lymphocytes are quantified as the readout of differentiation potentials (Figure S1I). Dynamic follow-up of lymphoid differentiation of LMDPs cultured under the standard SCF condition confirmed that, conversely to their $CD127^-$ counterparts that emerge within the first 48-h of culture, $CD127^+$ ELPs are detected only from culture-day 5, reaching maximum levels between culture days 7–10 (Figure 1D). To examine whether their delayed emergence reflects time-dependent changes in their lymphoid potential, LMDPs isolated earlier from xenografted mice (week-3) and cultured under the standard SCF condition, were sorted again by FACS on culture-days 2 or 5 and seeded for 5 or 2 more days in secondary cultures before comparative assessment of $CD127^{-/+}$ ELP output (Figure 1E). As expected, relative to their counterparts directly isolated from the BM of xenografted mice, day-2 and -5 LMDPs expanded less but produced increasing amounts of $CD127^+$ ELPs (Figures 1F and 1G). To ascertain that $CD127^-$ and $CD127^+$ ELPs differentiate independently, $CD45RA^{hi}CD127^-$ HPCs were next partitioned based on ITGB7 levels before seeding under diversification conditions (Figure 1H). Side-by-side comparisons confirmed that $CD127^-$ and $CD127^+$ ELPs differentially emerge from the more immature $ITGB7^-$ LMDP fraction (Figure 1I).

To test the *in vivo* relevance of these observations, LMDPs sorted at weekly endpoints from HSC-engrafted mice were seeded previously for 7 or 14 days under diversification conditions (Figure 2A). FACS analyses at day-7 confirmed that, in contrast to the stable production of monocyte and dendritic cells, lymphoid outputs follow an ascendant trend driven by the gradual increase in $CD127^+$ ELP production levels (Figure 2B) accompanied by a concordant increase in $CD19^+$ BLs at day-14 (Figure 2C). As expected, the lymphoid potential of self-renewed LMDPs sorted from LMDP-engrafted mice evolved in the same way (Figures S2C–S2F). To further document this point, we optimized the diversification assay by adding GM-CSF and TPO to SCF to readout the lympho-myeloid potential at a clonal resolution (Figure S1J). Analysis of clones derived from single HSCs or LMDPs sorted previously at weekly endpoints from HSC-engrafted mice showed that cloning efficiencies and expansion rates remain stable throughout the 5-week follow-up period (Figures S2G–S2J). Stratification according to lineage output confirmed that the HSC compartment (Figures 2D and S2K upper) comprises a majority of multipotent progenitors (MPPs) and revealed that granulomonocytic progenitors (GM) reach maximum levels during the first 2-week after grafting. Analysis of downstream LMDP compartment (Figures 2E and S2K lower panel) disclosed the expected enrichment in bior uni-lineage lymphoid or dendritic progenitors and found that, except for a late increase in dendritic progenitors, its clonal architecture remains stable over time. Again, focusing on ELP output revealed that, irrespective of their HSC or LMDP origin and, most importantly, independent of overall lymphoid potential, beyond the

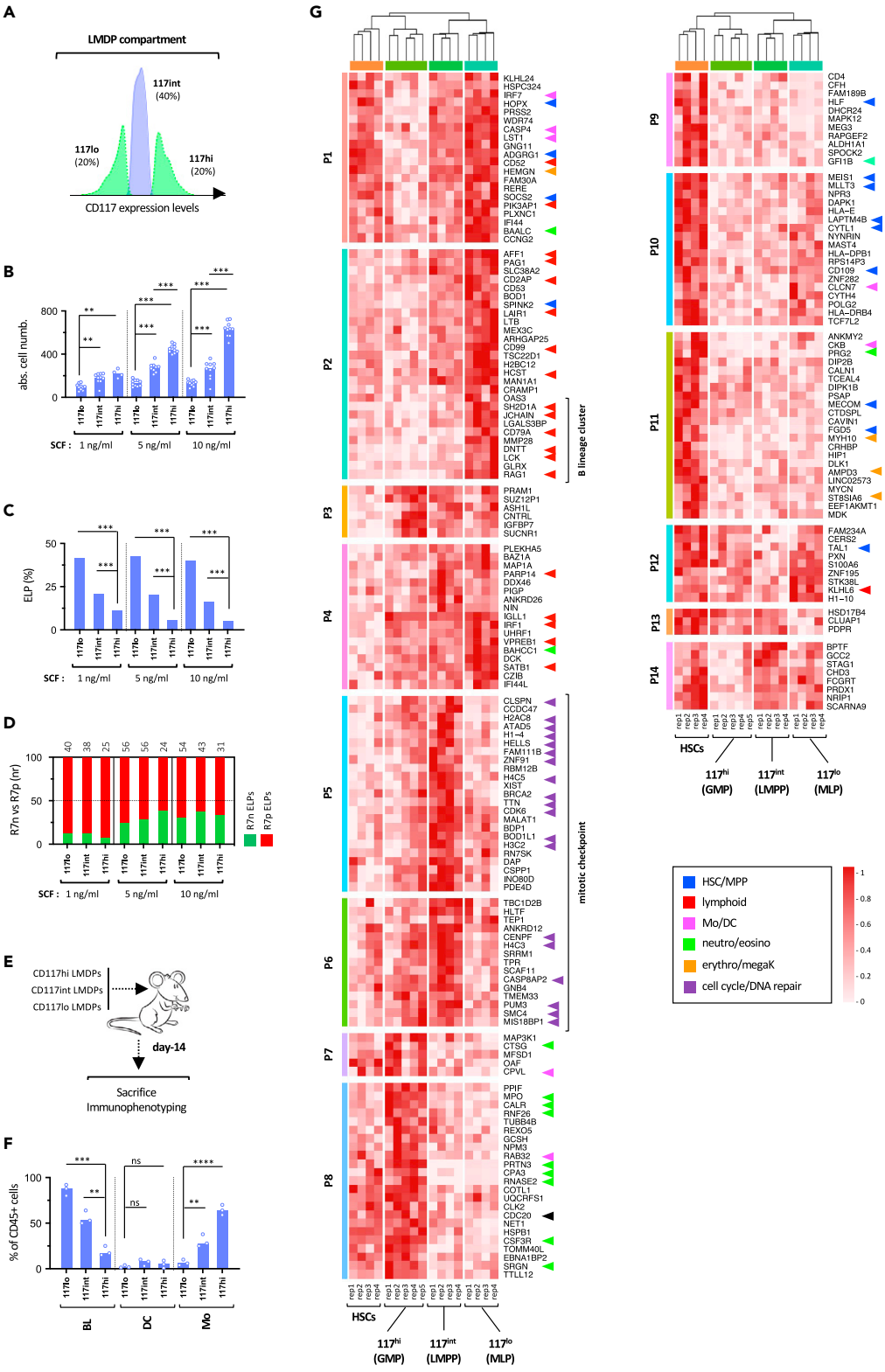
A
LMDP compartment
117int (40%)
117lo (20%)
117hi (20%)
CD117 expression levels
B
abs. cell numb.
SCF : 1 ng/ml 5 ng/ml 10 ng/ml
C
ELP (%)
SCF : 1 ng/ml 5 ng/ml 10 ng/ml
D
R7n vs R7p (nr)
R7n ELPs
R7p ELPs
SCF : 1 ng/ml 5 ng/ml 10 ng/ml
E
CD117hi LMDPs
CD117int LMDPs
CD117lo LMDPs
day-14
Sacrifice
Immunophenotyping
F
% of CD45+ cells
BL
DC
Mo
G
P1
P2
P3
P4
P5
P6
P7
P8
P9
P10
P11
P12
P13
P14
B lineage cluster
mitotic checkpoint
HSCs
117hi (GMP)
117int (LMPP)
117lo (MLP)
HSC/MPP
lymphoid
Mo/DC
neutro/eosino
erythro/megaK
cell cycle/DNA repair

Figure 3. Molecular and functional characterization of the CD117$^{hi\text{-}int\text{-}lo}$ LMDP fractions

(A) Immunophenotypic fractionation of LMDPs based on CD117 expression levels. The full gating procedure in shown in Figure S1A.

(B–D) *In vitro* assessment of the lymphoid potential of CD117$^{high,\ int,\ low}$ fractions. The indicated subsets were sorted at week-3 from the BM of HSC-xenografted mice and seeded by 100 cell/pools for 7 days in diversification assays supplemented with increasing doses of SCF.

(B) Absolute cell yields; bars indicate median cell number; circles correspond to individual wells.

(C) Percentages of CD127$^{-/+}$ ELPs; results are normalized relative to total hu-CD45^{+} cells; bars indicate medians.

(D) Stacked bar plots show normalized ratios of CD127^{-} (green) vs. CD127^{+} (red) ELPs. Results are expressed as median percentages of 15 replicates from one representative experiment; median numbers of ELPs per well are indicated (upper row). Assessment of statistical significance was performed with the Mann-Whitney test (****$p < 0.0001$; ***$p < 0.001$; **$p < 0.01$).

(E and F) *In vivo* assessment of the lymphoid potential of CD117$^{high,\ int,\ low}$ fractions.

(E) Experimental design: the indicated subsets were sorted as aforementioned from the BM of HSC-xenografted mice and transferred to secondary recipients (2×10^3 cell/mouse); recipient mice were sacrificed at week-2 after grafting.

(F) Bar plot showing the relative percentages of monocytes (Mo), dendritic cells (DC) or lymphoid cells among hu-CD45^{+} BM cells in mice reconstituted with of CD117$^{high,\ int,\ low}$ LMDPs; results are expressed as median percentages of the indicated cell subsets. Assessment of statistical significance was performed as aforementioned.

(G) Transcriptional profiling of the CD117$^{high,\ int,\ low}$ fractions. Heatmap showing expression of 207 selected DEGs across 14 clusters; gene expression values are log-transformed, normalized, and scaled; colored arrows show lineage- or subset-specific genes. Note that based on gene signatures the CD117$^{high,\ int,\ low}$ fractions are, respectively, referred to as GMPs, LMPPs, and MLPs. Flowchart summarizing the filtration and clustering strategies used for extraction of population-specific gene signatures are presented in Table S2A.

2nd week after grafting lymphoid-containing clones are increasingly biased toward the CD127^{+} ELPs (Figures 2F and 2G), consistent with the previous results.

To examine whether time-dependent variation in CD127^{-} and CD127^{+} ELP production pattern depends on the division history of their precursors, HSCs or LMDPs isolated at day 8 from mice reconstituted with CFSE-labeled HSCs or LMDPs were sub-fractionated according to the number of conservative divisions they had undergone (<4 versus > 5 divisions) and seeded previously in clonal assays (Figures 2H, S2L, and S2M). Quantification of ELP output confirmed that HSC or LMDPs which had undergone a higher number of previous cell divisions show a marked bias toward the production of CD127^{+} ELPs (Figures 2I–2K).

Collectively, these results indicate that the rise in CD127^{+} ELP production over time reflects qualitative changes in the lymphoid potential of HSC or LMDPs, independently of the duration of their stay in the bone marrow of xenografted mice.

CD127^{-} and CD127^{+} ELPs differentiate from bipotent CD117^{lo} MLPs

The finding that LMDPs comprise lymphoid progenitors led us to prospectively isolate candidate MLPs. Further immunophenotypic stratification revealed that decreasing CD117 expression levels coincides with downmodulation of myeloid CD33 (Figure S3A). To test whether lymphoid specification can be delineated on these bases, LMDPs were subdivided into three CD117$^{hi\text{-}int\text{-}lo}$ fractions before seeding in bulk diversification assays with graded doses of SCF (Figures 3A–3C). Downmodulation of CD117 correlated with the rise in lymphoid potential as well as concomitant decline in the cell expansion rates. Also, independently of overall lymphoid production and CD117 expression levels, low doses of SCF skewed lymphoid differentiation toward the CD127^{+} ELPs and the B lineage confirming their B-lineage bias (Figure 3D). To ascertain the physiological relevance of these results, CD117$^{hi\text{-}int\text{-}lo}$ LMDP fractions were transferred to irradiated mice (Figure 3E). Analysis of hu-CD45^{+} BM cells 2 weeks after grafting confirmed that the CD117^{lo} fraction retains only marginal myeloid differentiation potential (Figures 3F and S3B).

To search for concordant gene signatures, CD117$^{hi\text{-}int\text{-}lo}$ LMDP fractions, as well as HSCs, were subjected to transcriptional profiling with an ultra-low-input mini-RNA-seq method. Pairwise comparisons followed by unsupervised gene and population clustering identified 207 differentially expressed genes (DEG) partitioned into 14 gene expression patterns (P1-14) (Figure 3G; Table S2). Functional analysis and pattern distribution confirmed that HSCs selectively express genes regulating quiescence (P1, P12: *SOCS2*, *TAL1*, *HOPX*)[37,38] or self-renewal (P9-10: *HLF*, *MLLT3*, *MEIS1*),[39] as well as early regulators of erythro-megakaryocytic differentiation (P11: *AMPD3*, *MYH10*). Consistent with enrichment in granulomonocytic potential, CD117^{hi} LMDPs overexpressed *CSF3R*, *MPO*, *PRTN3* and *CTSG* (P7-8). As expected, decreasing CD117 expression coincided with extinction of granulomonocytic genes and concomitant upregulation of early lymphoid regulators (P2-4: *AFF1*, *SATB1*, *IRF1*) and lymphoid lineage genes (P2-4: *LAIR1*, *CD2AP*, *IGLL1*, *HSCT*, *VPREB1*) whose expression levels peaked in the CD117^{lo} fraction. Consistent with their intrinsic B-lineage bias, lymphoid-committed CD117^{lo} LMDPs displayed further overexpression of *JCHAIN*, *CD79A*, *DNTT*, and *RAG1* transcripts (P2, bottom). Genes involved in cell-cycle-related pathways (P5-6: DNA replication/repair, G2M mitotic checkpoint) were highly enriched in the CD117^{int} LMDP fraction suggestive of active proliferation. Expression of these genes dramatically decreased in downstream CD117^{lo} compartment, consistent with their low expansion rates. Importantly, CD117^{lo} LMDPs also retained (or upregulated) a repertoire of stem cell-associated genes (P1-10-12: *MEIS1*, *MLLT3*, *TAL1*, *HOPX*, *SOCS2*).

Consistent with our recent results,[30] these data demonstrate that downmodulation of CD117 coincide with gradual commitment toward the lymphoid lineage. In keeping with the current nomenclature, CD117 $^{hi\text{-}int\text{-}lo}$ LMDP fractions are thereafter referred to as CD117^{hi} granulomonocyte (GMP), CD117^{int} lymphoid-primed multipotent (LMPP), and CD117^{lo} multi-lymphoid (MLP) progenitors.

CD127^{-} and CD127^{+} ELPs are subject to divergent regulatory mechanisms

To further investigate the signaling pathways regulating the dichotomic choice between CD127^{-} and CD127^{+} ELPs, the same fractions were seeded in bulk under diversification conditions supplemented with lymphoid or myeloid growth factors (Figures 4A–4D). FACS analysis at

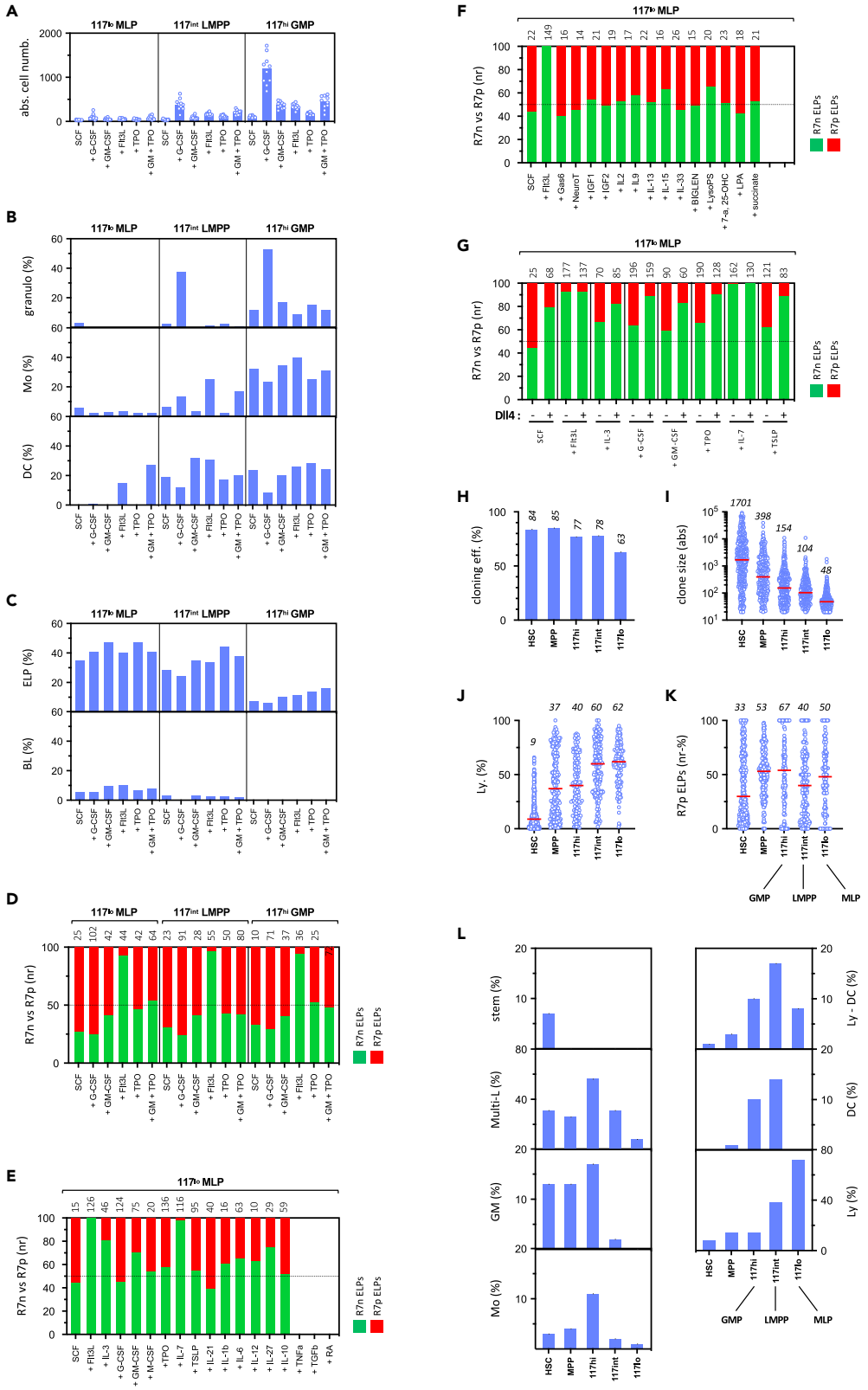
A
B
C
D
E
F
G
H
I
J
K
L
abs. cell numb.
granulo (%)
Mo (%)
DC (%)
ELP (%)
BL (%)
R7n vs R7p (nr)
cloning eff. (%)
clone size (abs)
Ly (%)
R7p ELPs (nr-%)
stem (%)
Multi-L (%)
GM (%)
Ly - DC (%)
R7n ELPs
R7p ELPs
GMP
LMPP
MLP

Figure 4. Effect of growth/differentiation factors on multi-lineage diversification

(A–D) The indicated CD117^{high} GMP, CD117^{int} LMPP, and CD117^{low} MLP fractions were seeded for 7 days by 100 cell-pools in diversification assays under the standard SCF condition (OP9 stroma) supplemented or not with the indicated growth factors before quantification of absolute cell yields and lympho-myeloid outputs.

(A) Shown are absolute cell yields; bars indicate median cell numbers; circles correspond to individual wells.

(B and C) Bar plots showing median percentages of (B) myeloid granulocytes (Granulo; upper panel), monocytes (Mo; medium panel), and dendritic cells (DC; lower panel) or of (C) lymphoid CD127$^{-/+}$ ELPs (upper panel) and BLs (lower panel) outputs.

(D) Stacked bar plots showing normalized ratios of CD127^{-} (R7n; green) vs. CD127^{+} (R7p; red) ELPs; results are expressed as median percentages of 5 to $\geq$ 20 replicates pooled from 3 independent experiments; median numbers of ELPs per well are indicated (upper row); positivity threshold for ELP detection is set arbitrarily at $\geq$ 10 ELPs/well).

(E–G) Functional screen of soluble regulators of CD127^{-} and CD127^{+} differentiation. CD117 ^{low} MLPs isolated as aforementioned from the BM of HSC-xenografted mice were cultured as aforementioned onto (E and F) OP9 or (G) OP9-DL4 stroma with the indicated ligands (all used at 1 ng/mL, except for RA: 10^{-5} M) before quantification of CD127^{-} and CD127^{+} ELP output. Stacked bar plot shows normalized ratios of CD127^{-} vs. CD127^{+} ELPs. For each growth/differentiation factor tested results are expressed as median percentages of 5 to $\geq$ 20 replicated pooled from at least 2 independent experiments. Positivity thresholds are defined as aforementioned; median numbers of ELPs per well are indicated.

(H–L) Clonal *in vitro* diversification assays. The indicated HSC (n = 550), MPP (n = 360), CD117^{hi} GMP (n = 570), CD117^{int} LMPP (n = 480), and CD117^{lo} MLP (n = 450) fractions were sorted from the BM of HSC-xenografted mice (week-3 post-grafting; see also Figure S1A for the gating procedure) and cultured for 14 days under the clonal *scf:gm-csf:tpo* condition (OP9 stroma) before quantification of lympho-myeloid output (see also legend of Figure 2).

(H) Upper left bar plot: cloning efficiency of corresponding cell fractions (positivity threshold: $\geq$ 20 cells/clone); percentages of positive clones are indicated (upper row).

(I) Upper right circle plot: absolute cell numbers per clone; median values are indicated (red bars; upper row).

(J) Lower left circle plot: percentages of lymphoid cells (Ly) per clone defined as the sum of the percentages of CD127$^{-/+}$ ELPs and CD19^{+} B cells; median values are indicated as aforementioned.

(K) Lower circle plot: relative percentages of CD127^{+} ELPs normalized relative to total ELP content on a per clone basis (positivity threshold for ELP detection is set arbitrarily at $\geq$ 10 ELPs/clone); median values are indicated.

(L) Bar plots showing percentages of stem (CD34^{+}Lin^{-}), granulomonocytic (GM), monocytic (M), multipotent (MPP), lympho-dendritic (Ly-DC), dendritic (DC) or lymphoid (Ly) clones across corresponding cellular fractions. Criteria used for clone stratification are described in the legend of Figure 2. Results are pooled from 2 independent experiments.

culture day-7 confirmed that CD117^{hi} GMPs display an exquisite susceptibility to G-CSF, whereas CD117^{int} LMPPs have mixed lympho-dendritic potential. Again, irrespective of culture conditions, CD117^{lo} MLPs expanded poorly and showed lymphoid-restricted output. With respect to ELP production patterns, this also revealed that, irrespective of cell compartment, adding TPO and/or GM-CSF results in balanced ELP outputs while supplementation in Flt3L induces a complete shift toward the CD127^{-} subset. To further document this point, CD117^{lo} MLPs were cultured onto OP9 or OP9-Dl4 stroma with SCF and 15 soluble ligands corresponding to growth/differentiation factors and pro- or anti-inflammatory cytokines (Table S3A; Figures 4E–4G). We found that as for Flt3L, Notch1 signaling favors CD127^{-} ELP differentiation from which a majority also upregulated surface CD7 indicative of T-lineage commitment. Supplementation in IL-7 also led to almost complete disappearance of the CD127^{+} subset. Analysis by multiplex PCR of in vitro-derived ELPs (Figure S3C; Table S3B) disclosed the expected fingerprints[36] within CD127^{-} (*MEF2C*, *RUNX2*, *IKZF1*, *ID2*, *NFIL3*) and CD127^{+} (*IL7R*, *RAG2*, *EBF1*, *FBXW7*) ELPs generated under SCF, TSLP, or Flt3L conditions, and confirmed that a 7-day culture on OP9-Dl4 stroma drives the emergence of prototypic T cell precursors (*DTX1*, *NOTCH3*, *LEF1*, *TOX*, and *CCR9*). Notably, CD127^{-} ELPs generated under the IL-7 condition downmodulated most lymphoid transcripts, including *CD127*. Inasmuch as this also resulted in a 4-fold increase in B cell output, we speculate that in presence of IL-7 B-cell differentiation bypasses the CD127^{+} ELPs. To screen for candidate inducers of CD127^{+} ELP differentiation, we finally tested the effect of 14 ligands of receptors whose transcripts are differentially expressed between LMDP and CD127$^{-/+}$ ELP fractions but, here again, with essentially negative results (Table S3A).

Subsequent analysis of 1,853 clones derived from 2,410 cells encompassing 5 consecutive compartments defined along a continuum of expression of CD45RA and CD117 found the expected decrease of median clone size as cells progress along the lymphoid differentiation axis and confirmed that ELP production patterns are largely independent of the ancestor cell type (Figures 4H–4K). Again, downmodulation of CD117 coincided with emergence of bior unipotent lymphoid or dendritic progenitors and then lymphoid-restricted MLPs (Figure 4L).

Collectively, these results show that CD127^{-} and CD127^{+} ELPs are subject to divergent Flt3L-dependent versus cell-autonomous regulatory mechanisms.

Flt3 signaling instructionally drives lymphoid differentiation toward the NK/ILC/T pathway

To decipher the gene regulatory networks controlling the choice between CD127^{-} and CD127^{+} ELPs, CD117^{lo} MLPs, CD117^{int} LMPPs, and CD117^{hi} GMPs, as well as HSCs were seeded for 6 h under the standard SCF condition with or without Flt3L or TPO before analysis by mini-RNA-seq (Figure 5A). Gene expression analyses based on global pairwise comparisons allowed selection of a compendium of 972 DEGs among which 638 Flt3L- and 544 TPO-responsive genes were identified (Table S4A). Side-by-side comparison between treated or untreated cellular subsets revealed that CD117^{lo} MLPs are the most responsive to Flt3L with 454 DEGs, as compared to 193 for CD117^{int} LMPPs and < 80 for the other HSC or CD117^{hi} GMPs (Figure 5B). Conversely to Flt3L, only minor differences were noted between TPO-treated CD117^{int} LMPPs and CD117^{lo} MLPs (281 versus 216 DEGs) (Figure 5C). Functional analysis of DEGs confirmed that in CD117^{lo} MLPs and to a lesser extent CD117^{int} LMPPs Flt3L induces a major developmental transition (Figure 5D; Tables S4B and S4C) which is characterized

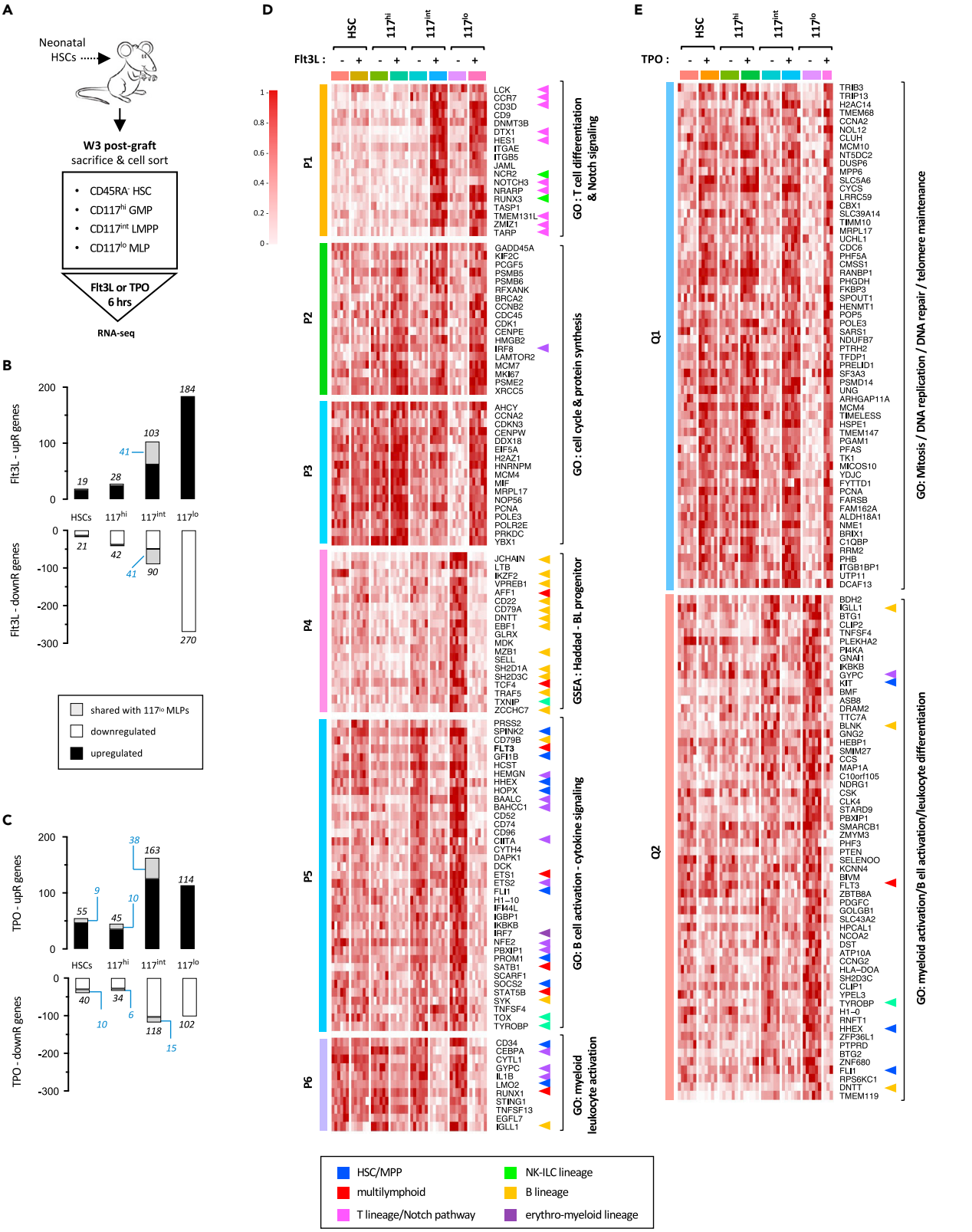
A
Neonatal HSCs
W3 post-graft
sacrifice & cell sort
CD45RA- HSC
CD117hi GMP
CD117int LMPP
CD117lo MLP
Flt3L or TPO
6 hrs
RNA-seq
B
Flt3L - upR genes
Flt3L - downR genes
HSCs
117hi
117int
117lo
shared with 117lo MLPs
downregulated
upregulated
C
TPO - upR genes
TPO - downR genes
D
Flt3L :
E
TPO :
P1
P2
P3
P4
P5
P6
GO : T cell differentiation & Notch signaling
GO : cell cycle & protein synthesis
GSEA : Haddad - BL progenitor
GO: B cell activation - cytokine signaling
GO: myeloid leukocyte activation
Q1
Q2
GO: Mitosis / DNA replication / DNA repair / telomere maintenance
GO: myeloid activation/B ell activation/leukocyte differentiation
HSC/MPP
multilymphoid
T lineage/Notch pathway
NK-ILC lineage
B lineage
erythro-myeloid lineage

Figure 5. Transcriptional response of CD117^{lo} MLPs to short-term stimulation with Flt3L or TPO

(A) Experimental design: the indicated HSC or CD117$^{hi, int, lo}$ GMP, LMPP and MLP subsets were seeded by 500 cell pools in 96-well plates and cultured for 6 h under SCF condition with or without Flt3L or TPO (10 ng/mL each) before being processed for mini-RNAseq.

(B and C) Barplots showing absolute numbers of (B) Flt3L- or (C) TPO-responsive genes; black and empty bars correspond respectively of up- or downmodulated genes; gray bars and blue numbers correspond to genes shared between CD117^{lo} MLPs and the other cell subsets.

(D and E) Heatmaps show expression of compendia of 120 (D) Flt3L- or (E) TPO-responsive genes within the indicated populations; gene expression values are log-transformed, normalized, and scaled; genes linked to Notch pathway, multi-lymphoid progenitors (blue) or T/NK- (green) or B- (red) or NK/ILC- (yellow) lineages are indicated. Flowchart summarizing the filtration and clustering strategies used for extraction of population- and condition-specific gene signatures are presented in Table S3A.

by upregulation of genes linked to NK/ILC/T differentiation (*LCK*, *NCR2*, *CD3*, *TARP*, *TMEM131L*, *CCR7*) or Notch signaling (*DTX1*, *HES1*, *Notch3*, *NRARP*) (P1), as well as of a broad repertoire of genes involved in cell cycle, DNA repair and protein synthesis pathways (P2-3). Concomitantly, genes controlling early lymphoid development (*AFF1*, *SATB1*, *RUNX1*) or B-lineage specification (*IKZF2*, *ETS1*, *EBF1*, *VPREB1*, *DNTT*, *JCHAIN*) (P4), as well as genes associated with stem/progenitor cell maintenance (*SOCS2*, *HOPX*, *LMO2*) or erythro-myeloid differentiation (*NFE2*, *GYPC*, *ETS2*, *GFI1B*, *CEBPA*, *IRF7*) (P5-6) were subjected to an active repression. Notably, Flt3L-treated cells also downmodulated *FLT3* transcripts, suggesting a potential negative auto-regulatory loop. In contrast, only minor differences in population-specific transcriptional responses were noted between TPO-treated subsets, stressing the specificity of the earlier results (Figure 5E; Tables S4D and S4E). Consistent with its established role in stem cell maintenance,[40] short-term stimulation with TPO resulted in upregulation of a wide repertoire of genes involved in DNA repair, telomere maintenance or cell cycle regulation (Q1) and corresponding downmodulation of *KIT* and *FLT3*, and diverse lineage marker genes (Q2: *IGLL1*, *BLNK*, *DNTT*, *GYPC*, *TYROBP*).

These results confirm that CD117^{lo} MLPs are hyper-responsive to Flt3L which instructionally drives their differentiation toward the NK/ILC/T pathway, while repressing their intrinsic B-lineage bias.

Increasing expression of B-lymphoid genes drives the dynamics of regenerative lymphopoiesis

To get further insight into the mechanisms controlling the dynamics of CD127^{+} ELPs in xenografted mice, we next searched for molecular correlates of the temporal variations in lymphoid production patterns described previously. Therefore, CD117^{lo} MLPs, CD117^{int} LMPPs, and CD117^{hi} GMPs as well as HSCs were sorted at weekly interval from HSC-xenografted mice and analyzed by mini-RNA-seq (Figure S4A). Pairwise comparisons across all time points and cell populations (76 pairwise comparisons) revealed a compendium of 2207 genes subjected to time-dependent variation and showed that they distribute in 5 predominant expression patterns (P1-5) (Table S5A; Figures S4B–S4E). Functional enrichment showed that the expression level of genes controlling cell proliferation, protein synthesis, or ATP metabolic processes peaks at week-1 after grafting (P1) to gradually decrease thereafter whereas genes involved in interferon signaling pathways (P2-4) follow an opposite upwards trend (Tables S5B–S5I). Consistent with the late expansion of DC progenitors detected previously, cell populations isolated from mice at week-5 after grafting overexpressed transcripts coding for regulators of DC differentiation (*IRF7*, *IRF8*, *SPIB*, *TCF4*) (P3-5). As expected, these analyses also revealed that over time HSCs upregulate a set of B-lymphoid genes correlating with the B-lineage polarization of their lymphoid output. Consistent with this observation, the repertoire of B-lymphoid genes subjected to time-dependent deregulation broadened as cells progressed along the lymphoid specification axis, reaching maximum diversity and expression levels in CD117^{lo} MLPs isolated from mice at week-5 after grafting. At that time, CD117^{lo} MLPs expressed at the highest levels *SATB1*, *MEF2A*, *EBF1*, *LEF1*, and *SOX4* TFs, as well as genes linked to IL-7 signaling (IL-*7R*, *JAK3*) and antigen receptor rearrangement (*ADA*, *DNTT*, *RAG1*), which here again was indicative of increasing specification toward the B lineage. These analyses also found that, in contrast to *CD3D* whose expression declined over time, *FLT3* transcript levels followed an upward trend which suggests that despite an increasing B-lineage bias CD117^{lo} MLPs remain fully responsive to Flt3L.

These data indicate that the temporal shift of lymphoid potential toward the CD127^{+} ELP subset is driven by increasing expression of B-lineage genes detectable as early as the level of HSCs, which reinforces the view that B-lymphoid potential is regulated cell-autonomously.

Single-cell transcriptional mapping identifies distinct MLP1 and MLP2 subsets

To characterize lymphoid differentiation trajectories at a clonal resolution, CD34^{hi} HSPCs from HSC-xenografted mice at week-3 were subdivided into four compartments including CD127^{-} and CD127^{+} ELPs before analysis by single-cell RNA sequencing (Figure S5A). This procedure ensures an equal representation of the corresponding cell fractions, thereby maximizing the capture of discrete cellular states. After quality control and doublet exclusion the final dataset was composed of 37,092 cells which were projected on a 2D space (UMAP) (Figures 6A and 6B). Graph-based Louvain clustering disclosed 20 clusters (C0-19) associated with 13 cell types identified based on a set of 42 manually selected lineage gene markers among the 3,844 DEGs (Figure 6C). Analysis of cluster-specific signatures (Table S6) confirmed the overexpression of genes involved in stem cell maintenance or self-renewal (*LMO2*, *HOPX*, *TIE1*, *MEIS1*, *MLLT3*) in HSCs (C1) and the expected enrichment in protein synthesis or oxidative phosphorylation pathways in downstream multipotent progenitors (MPP1/2; C2-3). MPPs also displayed evidence of differential lymphoid (MPP1 [C2]: *AFF1*, *SATB1*, *FLT3*) versus myeloid (MPP2 [C3]: *CEBPA*) transcriptional priming. Granulomonocytic progenitors (GMP1-2; C4-5) overexpressed *KIT* transcripts and granulocytic lineage genes (*CEBPA*, *CSF3R*, *MPO*, *ELANE*), while subsequent individualization of lineage-specified monocyte precursors (C7) was associated with the upregulation of *CSF1R*, *CEBPD*, *IRF8*, or *SAMHD1*. Eosinophil/basophil/mast cell progenitors (EBMP; C6: *GATA1*, *GATA2*, *CEBPE*, *IL5RA*) remained confined to the CD45RA$^{-/int}$ compartment (Figure S5B) indicating their independent differentiation.[34] Consistent with the mini-RNA-seq data, enrichment analyses

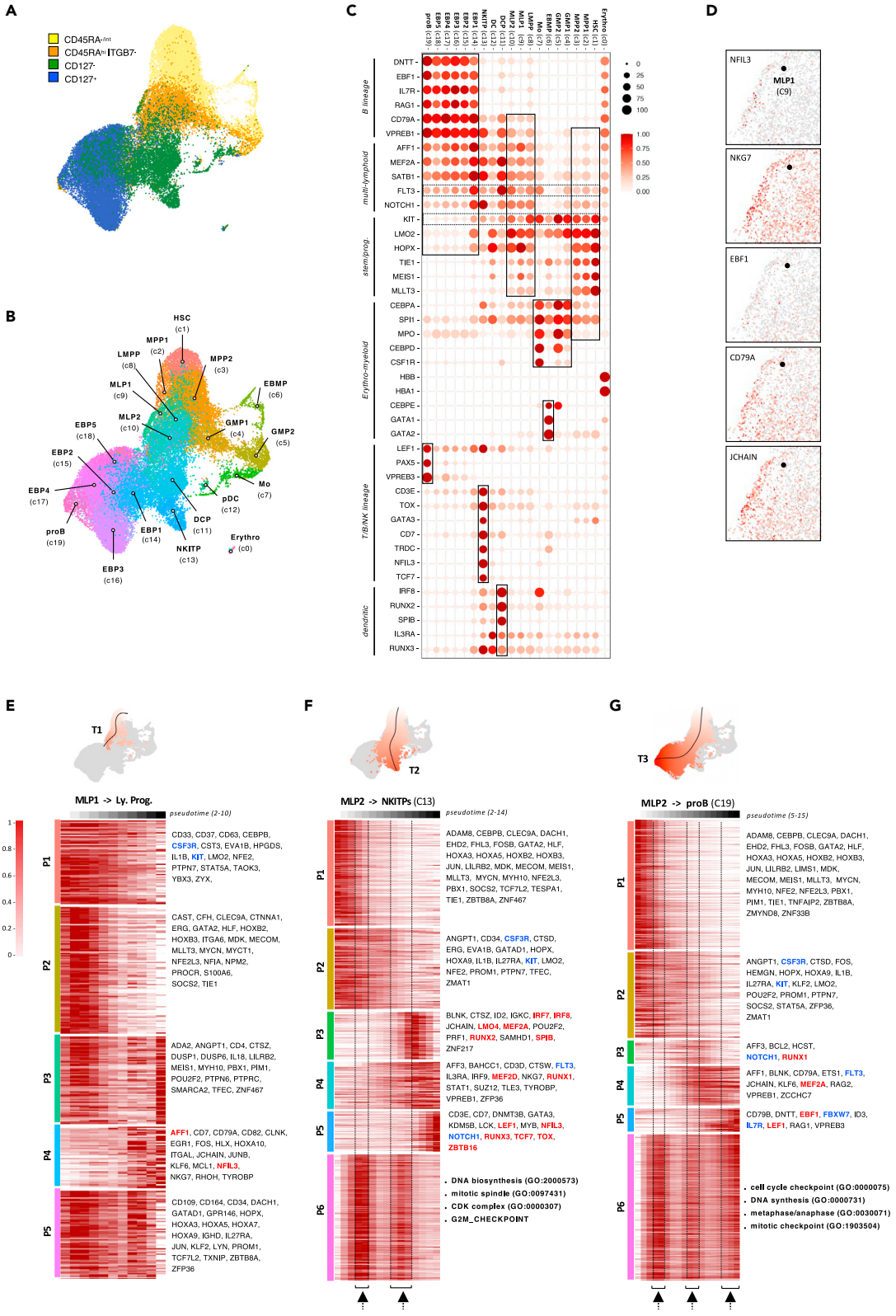
A
CD45RA-int
CD45RAhi ITGB7-
CD127-
CD127+
B
HSC (c1)
MPP1 (c2)
MPP2 (c3)
LMPP (c8)
MLP1 (c9)
MLP2 (c10)
EBMP (c6)
GMP1 (c4)
GMP2 (c5)
EBP5 (c18)
EBP2 (c15)
EBP4 (c17)
proB (c19)
EBP1 (c14)
EBP3 (c16)
NKITP (c13)
DCP (c11)
pDC (c12)
Mo (c7)
Erythro (c0)
C
B lineage
multi-lymphoid
stem/prog.
Erythro-myeloid
T/B/NK lineage
dendritic
D
NFIL3
MLP1 (C9)
NKG7
EBF1
CD79A
JCHAIN
E
T1
MLP1 -> Ly. Prog.
pseudotime (2-10)
F
T2
MLP2 -> NKITPs (C13)
pseudotime (2-14)
G
T3
MLP2 -> proB (C19)
pseudotime (5-15)
DNA biosynthesis (GO:2000573)
mitotic spindle (GO:0097431)
CDK complex (GO:0000307)
G2M_CHECKPOINT
cell cycle checkpoint (GO:0000075)
DNA synthesis (GO:0000731)
metaphase/anaphase (GO:0030071)
mitotic checkpoint (GO:1903504)

Figure 6. Analysis of lymphoid differentiation trajectories by scRNA-Sequencing

The indicated CD45RA$^{-/int}$, CD45RA^{hi}ITGB7^{-}, and CD127^{-} or CD127^{+} HSPC subsets were isolated from the BM of HSC-xenografted mice (week-3) and subjected to scRNA-seq profiling with the 10X genomic platform (see also Figure S5A).

(A and B) UMAP visualization of the compendium of CD34^{+} HSPCs colored by (A) cellular compartment or (B) cell clusters (c0-19) annotated based on expression of canonical lineage marker genes for hematopoietic stem cells (HSC: C1), multipotent progenitors (MPP: C2-3), granulomonocytic progenitors (GMP: C4-5), eosinophil/basophil/mast cell progenitors (EBMP: C6), monocytes (Mo: C7), lympho-primed multipotent progenitor (LMPP: C8), multi-lymphoid progenitors (MLP: C9-10), dendritic cell precursors (DCP: C11), plasmacytoid dendritic cells (pDC: C12), NK/ILC/T progenitors (NKITP: C13), early B cell precursors (EBP: C14-18) or pre-pro-B cells (pre-pro-B: C19), erythroid progenitors (Erythro: C0); circles correspond to medoids.

(C) Spot plot based on expression of 42 arbitrarily selected genes show lineage fingerprints of clusters C1-19; dashed areas show cluster-specific gene signatures.

(D) UMAP visualization of lymphoid NK/ILC (*NFIL3*, *NKG7*) or B (*CD79A*, *JCHAIN*, *EBF1*) lineage genes in individual cells along the MLP1 differentiation trajectory; black dot corresponds to MLP1 medoid (C9).

(E–G) Variations along pseudotime of transcriptional programs of lymphoid (E) MLP1- or MLP2-based (F) NKIT or (G) differentiation trajectories. Upper UMAPs show corresponding differentiation trajectories represented as smoothed black curves; lineage-specific cells are color-coded (white to red) according to pseudotime values. Heatmaps represent min to max normalized expression of dynamically variable genes; trajectory inference analyses were performed with SlingShot. Growth factor receptors are in blue; TFs are in red; GO/GSEA enrichments are indicated. Dashed lines and black arrows correspond to cell proliferation phases.

confirmed upregulation of pre-BCR components in actively cycling CD117^{int} LMPPs (C8) (Figure S5C). Most importantly, these analyses allowed the identification of distinct MLP1 (C9) and MLP2 (C10) clusters with largely overlapping G1 cell-cycle statuses and gene signatures (*AFF1*, *MEF2A*, *SATB1*, *FLT3*, *CD79A*, *VPREB1*), but distant projection on the transcriptional space. Whereas MLP2s (C10) displayed a spatial promiscuity with LMPPs (C8) suggestive of precursor-successor relationships, MLP1s expressed at higher levels stem cell-associated transcripts (*HOPX*, *TIE1*, *MEIS1*, *MLLT3*) and projected in close association with cells overexpressing NK/ILC (*NFIL3*, NKG7) or B (*EBF1*, *CD79A*, *JCHAIN*) lineage genes (Figure 6D).

Louvain clustering allowed subdivision of downstream CD127^{+} ELPs into immature early B cell progenitors (EBP1; C14) displaying a dual multi-lymphoid (*FLT3*, *SATB1*, *AFF1*, *MEF2A*) and B-lineage (*IL7R*, *EBF1*, *SOX4*, *ZCCHC7*, *RAG2*, *DNTT*) gene signature, and four prototypic EBP2-5 subsets (C15-18), all converging toward pro-B cells (C19: *LEF1*, *PAX5*, *VPREB3*). As expected,[36] NK/ILC/T progenitors (NKITP; C13) overexpressed NK-ILC (*ID2*, *NFIL3*, *TOX*, *LMO4*) or T (*LEF1*, *TCF7*, *GATA3*, *TRDC*, *CD3E*) lineage genes and were exclusively situated within the CD127^{-} compartment. Most immature dendritic cell progenitors (DCP) (C11: *IRF8*, *RUNX2*, *SPIB*, *FLT3*, *IL3R*) retained expression of B-lymphoid genes (*IGKC*, *BLNK*, *IGHM*, *JCHAIN*) stressing their developmental promiscuity with the lymphoid lineage. Analysis of expression of 12 lineage-specific genes in individual cells (Figure S5D) finally revealed that whereas *IGHM/D* transcripts are detected as early as the HSC level, the expression of genes affiliated to NK/ILC or T lineages (*TRD, NFIL3*, *TCF7*, *GATA3*) remains confined to downstream NKITPs (C13) which, here again, was consistent with discrepant cell-intrinsic versus inducible regulatory modes. As expected, expression of *PAX5*, *CD24*, or *VPREB3* was largely confined to the pro-B cluster (C19) area.

MLP1s and MLP2s determine independent lymphoid pathways

SlingShot analyses[41] were next performed to calculate pseudotime and delineate lymphoid differentiation paths. Lineage reconstruction revealed 1 MLP1- (T1) and 4 MLP2-based (T2-5) differentiation trajectories (Figure S6A; Table S7). Cluster analysis showed the dynamic upregulation of lymphoid lineage genes (P4) along the T1 MLP1-based path and confirmed persistent expression of stem cell-associated genes (P3-P5), suggestive of direct emergence from HSCs (Figure 6E). This contrasted with alternate MLP2-based T2-5 trajectories along which lymphoid specification begins with sequential downmodulation of stem/progenitor (P1) and erythro-myeloid lineage (P2) genes and continues with the proliferative burst of LMPPs followed by the proliferation arrest (P6) of MLPs preceding the separation between NKIT- and B-lineages. Dissection of CD127^{-} NKIT differentiation pathway (T2) (Figure 6F) revealed a single wave of proliferation (P6) followed by upregulation of NK/ILC (*TOX*, *NFIL3*, *ZBTB16*) and then T lineage genes (*LEF1*, *TCF7*, *CD3E*) (P5). Analysis of CD127^{+} differentiation trajectories (T3-5) revealed that B cell progenitors undergo two rounds of proliferation, with the first wave of expansion driving progression toward EBP1s whose proliferation arrest coincided with repression of *NOTCH1* and *FLT3* and corresponding increase in *IL7R* and *FBXW7* transcripts (Figures 6G, S6B, and S6C). Also, in contrast to T4 and T5 trajectories that moved toward proliferative EBP3-5 clusters, the T3 trajectory ran into the pro-B cluster (C19) and therefore corresponded to the canonical B cell differentiation pathway. Lineage reconstructions confirmed the developmental promiscuity between lymphoid and dendritic lineages and showed that along the DC differentiation path *IL3R* upregulation precedes segregation into plasmacytoid or conventional DC subsets (Figures S7A and S7B). Subsequent analysis of granulocyte (T7) or monocyte (T8) trajectories revealed that, unlike their lymphoid or dendritic counterparts, myeloid lineage cells follow essentially continuous pathways driven by gene differentiation and proliferation modules operating in a combinatorial manner (Figures S7C and S7D).

Collectively, these data confirm that MLP1s and MLP2s determine independent lymphoid pathways and show that MLP2-based differentiation trajectories are specified by alternating phases of cell proliferation and differentiation.

CD117^{lo} MLPs emerge via direct or stepwise differentiation pathways

A lentiviral barcoding approach was finally applied to trace the origin of CD117^{lo} MLPs and follow their differentiation in the BM of xenografted mice (Figure 7A). Analysis of the repertoire of barcodes distributed across 8 HSC, myeloid (GMP, Mo prec., DC prec.) or lymphoid (MLP, CD127$^{-/+}$ ELP, pro-B) compartments allowed detection of 1,490 unique barcodes (Table S8), of which only 179 (12%) were present

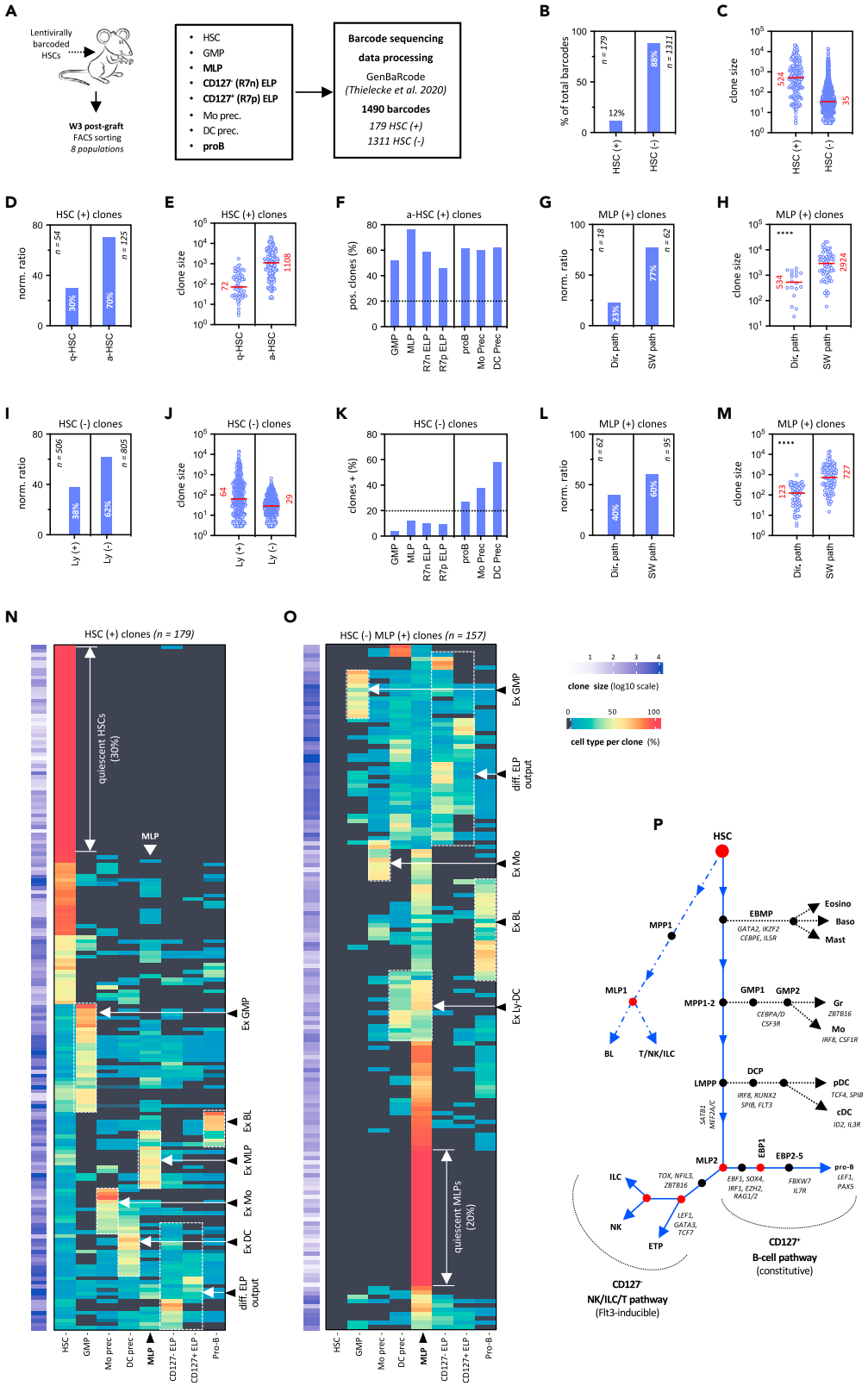
A
Lentivirally barcoded HSCs
W3 post-graft
FACS sorting
8 populations
HSC
GMP
MLP
CD127- (R7n) ELP
CD127+ (R7p) ELP
Mo prec.
DC prec.
proB
Barcode sequencing data processing
GenBaRcode
(Thielecke et al. 2020)
1490 barcodes
179 HSC (+)
1311 HSC (-)
B
% of total barcodes
n = 179
n = 1311
12%
88%
HSC (+)
HSC (-)
C
clone size
524
35
D
HSC (+) clones
norm. ratio
n = 54
n = 125
30%
70%
q-HSC
a-HSC
E
HSC (+) clones
clone size
72
1108
F
a-HSC (+) clones
pos. clones (%)
GMP
MLP
R7n ELP
R7p ELP
proB
Mo Prec
DC Prec
G
MLP (+) clones
norm. ratio
n = 18
n = 62
23%
77%
Dir. path
SW path
H
MLP (+) clones
clone size
****
534
2924
I
HSC (-) clones
norm. ratio
n = 506
n = 805
38%
62%
Ly (+)
Ly (-)
J
HSC (-) clones
clone size
64
29
K
HSC (-) clones
clones + (%)
L
MLP (+) clones
norm. ratio
n = 62
n = 95
40%
60%
M
MLP (+) clones
clone size
****
123
727
N
HSC (+) clones (n = 179)
quiescent HSCs (30%)
MLP
Ex GMP
Ex BL
Ex MLP
Ex Mo
Ex DC
diff. ELP output
HSC
GMP
Mo prec.
DC prec.
MLP
CD127- ELP
CD127+ ELP
Pro-B
O
HSC (-) MLP (+) clones (n = 157)
Ex GMP
diff. ELP output
Ex Mo
Ex BL
Ex Ly-DC
quiescent MLPs (20%)
clone size (log10 scale)
cell type per clone (%)
P
HSC
MPP1
EBMP
GATA2, IKZF2
CEBPE, IL5R
Eosino
Baso
Mast
MLP1
BL
T/NK/ILC
MPP1-2
GMP1
GMP2
CEBPA/D
CSF3R
Gr
ZBTB16
Mo
IRF8, CSF1R
LMPP
DCP
IRF8, RUNX2
SPIB, FLT3
pDC
TCF4, SPIB
cDC
ID2, IL3R
SATB1
MEF2A/C
MLP2
EBP1
EBP2-5
pro-B
LEF1, PAX5
FBXW7
IL7R
EBF1, SOX4, IRF1, EZH2, RAG1/2
ILC
TOX, NFIL3, ZBTB16
NK
LEF1, GATA3, TCF7
ETP
CD127+
B-cell pathway
(constitutive)
CD127-
NK/ILC/T pathway
(Flt3-inducible)

Figure 7. CD117^{lo} MLPs arise from distinct direct or stepwise differentiation pathways

(A) Experimental design: neonatal HSCs (CD34^{hi}CD45RA^{-}CD38$^{lo/-}$Lin^{-}) were transduced (6-h exposure) with a library of barcoded *egfp*-reporter lentiviruses (transduction efficiency < 30%) before intravenous injection to irradiated NSG mice (2 × 10^{5} cells/mouse). Recipient mice were sacrificed as aforementioned at week-3 after grafting before the indicated hu-CD45^{+}egfp^{+} multipotent (HSC), lymphoid (MLP, ELP, pro-B; bold characters) or myeloid (GMP, Mo prec., DC prec.) subsets were FACS-sorted and processed for analysis of barcode repertoires.

(B and C) Distribution of barcodes between HSC (+) and HSC (–) clones.

(B) Right barplot shows percentages of active (HSC [+]) vs. exhausted HSCs (HSC [-]).

(C) Circle plot shows absolute barcode numbers per HSC (+) or HSC (–) clone (referred to as "clone size"); red bars indicate medians; corresponding values are indicated. HSC (+) clones: ≥ 1 copy of a unique barcode detected within the HSC compartment.

(D–H) Lineage output of HSC (+) clones.

(D) Barplot showing relative percentages of active (a) or quiescent (q) HSC (+) clones (active clone: ≥ 1 copy of a unique barcode detected within lymphoid or myeloid subsets).

(E) Circle plot showing absolute barcode numbers per active (left panel) or quiescent (right panel) clone.

(F) Immunophenotypic stratification of aHSC (+) clones: barplot showing percentages of aHSC (+) clones positive for each the indicated subset (positivity threshold: ≥ 1 copy per compartment).

(G) Barplot showing the relative proportions of MLP (+) clones arising through the direct (Dir) or stepwise (SW) differentiation pathways (MLP (+) clones: ≥ 1 copy of a unique barcode detected within the MLP compartment).

(H) Circle plot shows absolute barcode numbers per Dir or SW MLP (+) clone. Percentages, median and absolute values are indicated.

(I–M) Lineage output of HSC (–) clones.

(I) Barplot showing relative proportions of Ly (+) vs. Ly (–) clones (Ly [+] clones: ≥ 1 copy of a unique barcode detected within lymphoid MLP, ELP, or pro-B compartments).

(J) Circle plot showing absolute barcode numbers per Ly (+) or Ly (–) clone.

(K) Immunophenotypic stratification of HSC (–) clones: barplot showing percentages of HSC (–) clones positive for each the indicated cell subset.

(L) Barplot showing the relative proportions of MLP (+) clones arising through the direct (Dir) or stepwise (SW) differentiation pathways.

(M) Circle plot shows absolute barcode numbers per Dir or SW MLP (+) clone. Percentages, median and absolute values are as aforementioned. Assessment of statistical significance was performed with the Mann-Whitney test (****$p < 0.0001$; ***$p < 0.001$; **$p < 0.01$).

(N and O) Heatmaps representation of the lineage output of (N) HSC (+) (n = 179) or (O) HSC (–) MLP (+) (n = 157) clones. Clustering uses complete linkage and Euclidian distance. Dashed areas show differentiation patterns. Diff. ELP output: differential ELP output. Color scales are arbitrarily set as "black" for "0" values.

(P) An integrated model of lymphopoiesis. Differentiation along the direct lymphoid pathway (MLP1; dashed blue line) proceeds in absence of multi-lineage diversification. Differentiation along the stepwise pathway (MLP2; plain blue line) follows the hematopoietic hierarchy with sequential emergence of EBMPs, GMP1-2 and then LMPPs. Following individualization of GMP1s, MPP1-2s start downmodulating CD117 to differentiate into CD117^{int} LMPPs. At this stage, cells undergo a proliferative burst also resulting in individualization of bior unipotent lymphoid or dendritic progenitors. Lymphoid restriction occurring at the level of CD117^{lo} MLP1-2s is associated with a proliferation arrest marking the first lymphoid development checkpoint. Subsequent dichotomic choice between the B (CD127^{+}) and T/NK/ILC (CD127^{-}) pathways relies on a dynamic balance between the intrinsic B-lineage bias of CD117^{lo} MLPs and extrinsic Flt3-signaling. Downstream progression along the CD127^{+} B-lymphoid pathway comprises a first phase of amplification presumably controlled by low levels of Notch1 and Flt3L signaling that drive progression until EBP1s whose subsequent proliferation arrest coincides with IL7R upregulation. Downstream EBP2-5 undergoes a second phase of IL7-dependent amplification also driving subsequent differentiation into PAX5^{+} pro-B cells. Differentiation along the T/NK/ILC pathway comprises a single wave of Flt3L-dependent proliferation followed by secondary diversification into NK, ILC, or T lineage-specified precursors exiting the BM to reach the thymus or secondary lymphoid organs. NK precursors become strictly dependent on IL-2/15 for subsequent differentiation; common ILC progenitors upregulate IL-7R and undergo secondary diversification into ILC1, ILC2 or ILC3 precursors; ETPs leave the BM to reach the thymus. Abbreviations: EBMP: eosinophil/basophil/mast cell progenitor; GMP: granulomonocytic progenitor; MPP: multipotent progenitors; LMPP: lymphoid-primed multipotent progenitor; DCP: dendritic cell progenitor; MLP: multi-lymphoid progenitor; ELP: early lymphoid progenitor; EBP: early B cell precursor; NK: natural killer; ILC: innate lymphoid cells; ETP: early T cell progenitor. Back and red circles indicate lineage branching points; red circles correspond to the cell cycle arrests proposed as developmental checkpoints.

within the HSC compartment [HSC (+)], indicating that 3 weeks after grafting the majority of the barcoded HSCs initially transplanted had reached functional exhaustion. Consistent with this view, HSC (+) clones were 15-fold larger than their HSC (–) counterparts (Figures 7B and 7C). Subsequent analyses unexpectedly revealed that 30% of HSC (+) clones have no detectable progeny, indicating their functional quiescence (qHSCs) (Figures 7D and 7E). As expected, clones derived from active HSCs (aHSCs) included a mixture of lymphoid or myeloid cellular subsets (Figure 7F). To further delineate the routes of differentiation of CD117^{lo} MLPs, we then focused on MLP-containing clones [MLP (+)] and found that 23% of them originate from HSCs with no detectable myeloid progeny, which was suggestive of direct differentiation (Figures 7G and 7H). Subsequent characterization of clones derived from exhausted HSCs confirmed that those containing lymphoid cells [Ly (+)] are 2-fold larger than their Ly (–) counterparts (Figures 7I and 7J), and disclosed the expected depletion in more immature GMP, MLP, or ELP subsets (Figure 7K). Again, a substantial proportion of MLP-containing clones had no detectable myeloid progeny (Figures 7L and 7M). Subsequent analysis of lineage relationships confirmed that across HSC (+) clones multi-lineage diversification follows the hematopoietic hierarchy, with expansion of myeloid granulocyte or monocyte coinciding with a decrease in dendritic or lymphoid output (Figure 7N). Also consistent with the *in vitro* clonal diversification data, the numbers of barcodes detected in dendritic precursors or CD117^{lo} MLPs varied in inverse proportions, reinforcing the view that segregation between lymphoid and dendritic lineage fates occurs at the level of common LMPP ancestors. As expected, MLP-containing clones displayed balanced or biased ELP output. Analysis of clones derived from exhausted

HSC largely confirmed these findings, but also revealed that 20% of MLPs have no detectable progeny, again suggesting functional quiescence (Figure 7O).

Overall, barcoding analyses confirm that CD117^{lo} MLPs emerge via direct or stepwise differentiation pathways but do not allow the MLP1 and MLP2 subsets to be formally assigned to either pathway.

DISCUSSION

In this study, combining time course and endpoint molecular and functional analyses with genetic barcoding in a humanized mouse model, we establish an updated cartography of human lymphopoiesis that extends the current view of lymphoid organization (Figure 7P).

As well as shedding a new light on the developmental relationships between lymphoid and myeloid lineages, our results demonstrate that previously characterized CD127^{-} and CD127^{+} ELPs[36] originate from a novel subset of canonical CD117^{lo} MLPs. Functional *in vitro* diversification assays showed that the dichotomic choice between CD127^{-} and CD127^{+} ELPs takes places at the level of CD117^{lo} MLPs and revealed that these populations are subject to discrepant FLT3L-inducible versus cell-intrinsic regulatory modes. Indeed, whereas Flt3 signaling instructionally drives CD117^{lo} MLPs toward the NK/ILC/T pathway, none of the factors tested in diversification assays could promote the emergence of B-lineage biased CD127^{+} ELPs. The proposition that entry into the B-lymphoid pathway is controlled cell-autonomously relies on several lines of evidence. Firstly, our data indicate that the time-dependent increase in CD127^{+} ELP production observed in xenografted mice is driven by a global B-lineage shift in the lymphoid potential of their precursors, which is also observed as an increase in expression of B-lymphoid genes detected as early as the HSC level. Secondly, we provide evidence that these changes are ultimately conditioned by the divisional history of CD34^{+} HSPCs, independent of their differentiation stage. Third, functional characterization of CD117^{lo} MLPs demonstrates that their intrinsic B-lineage bias is counterbalanced by acquisition of an exquisite susceptibility to Flt3L, finding consistent with a recent study from our group[30] as well as with earlier reports in the mouse.[16,42,43] Given that a similar time-dependent rise in CD127^{+} ELP production is observed during the recovery phase in pediatric patients treated with chemotherapy for acute leukemia,[30] the gradual polarization of lymphoid production pattern toward the B lineage described here likely represents an intrinsic feature of regenerative lymphopoiesis.

Transcriptional profiling of CD34^{hi}CD45RA^{hi} HSPCs confirmed that lymphoid priming begins in actively proliferating CD117^{int} LMPPs where separation between lymphoid and dendritic lineages also occurs.[44] Lymphoid commitment of CD117^{lo} MLPs was associated with an active repression of myeloid genes and corresponding upregulation of genes coding early lymphoid regulators. Most importantly, consistent with limited growth factor responsiveness, CD117^{lo} MLPs downmodulated most genes involved in cell-cycle-related pathways indicating that a proliferation arrest precedes the dichotomic choice between CD127^{-} and CD127^{+} lymphoid pathways. Analyses of cluster-specific genes signatures revealed in addition that, like their counterparts from the neonatal cord blood,[30] CD117^{lo} MLPs overexpress a repertoire of stem cell-associated genes. Although the extent to which persistence of these genes influences their biological properties remains elusive, we speculate that this could reflect an imprint left by their upstream precursors (particularly when they arise from the direct pathway) or indicate that lymphoid restriction is associated with acquisition of some stem cell-like properties, such as functional quiescence and a certain degree of self-renewal. This assumption is supported by the barcoding data showing that functionally quiescent CD117^{lo} MLPs are detected in the BM of xenografted mice. Finally, based on shared immunophenotypic, functional and molecular profiles, CD117^{lo} MLPs could be considered as human counterparts of recently described mouse CD117^{lo}FLT3^{hi} LPPs.[17] Given the evidence that, in the mouse embryo, early T-lineage progenitors (ETPs) also differentiate independently of CD127^{+} CLPs,[45–47] this suggests that the bipartite organization of lymphoid development architecture is conserved across species.[36]

Single-cell transcriptional analyses unexpectedly revealed that CD117^{lo} MLPs segregate into distinct (but phenotypically indistinguishable) MLP1 and MLP2 clusters with distant projection on the transcriptional space and differential expression of stem cell genes. Lineage reconstruction confirmed that newly described MLP1 and MLP2 subsets determine independent differentiation pathways. Whereas MLP1s emerge directly from HSCs in absence of multilineage diversification, MLP2 differentiation follows a stepwise differentiation pathway characterized by early separation of granulomonocytic lineage fates, followed by individualization of bipotent lympho-dendritic LMPPs and then downstream segregation into unipotent dendritic or lymphoid progenitors. Analyses of *in vivo* cell fates by cellular barcoding confirmed that lymphoid specification proceeds via independent direct or stepwise differentiation pathways but did not allow MLP1s and MLP2s to be formally assigned to either pathway. Therefore, whether MLP1s and MLP2s are functionally redundant, or display subset-specific properties is currently unclear and clearly deserves further investigation. In silico reconstruction of lineage trajectories finally revealed that, unlike granulomonocytic differentiation that proceeds in an essentially continuous manner along which cell growth, proliferation and differentiation remain intimately linked,[48,49] lymphoid differentiation trajectories are intrinsically discontinuous and comprise alternating phases of proliferation and differentiation. Cluster-specific signatures confirmed that while phases of cell expansion allow pre-commitment amplification of lymphoid progenitor pools, intervening proliferative arrests mark key transitions in cell differentiation status and growth factor dependencies, also suggesting that they may correspond to previously undescribed checkpoints of lymphoid development.

Limitations of the study

Although most of the findings reported in the currently study have been recently validated on primary CD34^{+} HSPCs isolated from placental blood or bone marrow from healthy donors,[30] the physiological relevance of other results still needs to be formally established. For example,

it remains unclear at present whether MLP1- or MLP2-based lymphoid pathways and newly described developmental checkpoints can also be observed under basal conditions in steady-state hematopoiesis. These issues should be the subject of future studies.

STAR★METHODS

Detailed methods are provided in the online version of this paper and include the following:

- KEY RESOURCES TABLE
- RESOURCE AVAILABILITY
  - Lead contact
  - Materials availability
  - Data and code availability
- EXPERIMENTAL MODELS AND STUDY PARTICIPANT DETAILS
  - Human sample collection
  - Mice
- METHODS DETAILS
  - Processing of human cord blood and cell separation
  - Xeno-transplantations
  - Flow cytometry and cell sorting
  - Cell cultures and analysis
  - Transcriptional profiling by multiplex PCR
  - Gene expression profiling by mini-RNA-seq
  - Single cell-RNA-seq
  - Lentiviral barcoding
- QUANTIFICATION AND STATISTICAL ANALYSIS
  - Mini-RNA-seq analysis
  - Single cell-RNA-seq analysis

SUPPLEMENTAL INFORMATION

Supplemental information can be found online at https://doi.org/10.1016/j.isci.2023.107890.

ACKNOWLEDGMENTS

The authors thank Christelle Doliger and Niclas Setterblad (Plateforme d'Imagerie et de Tri Cellulaire, IRSL, Paris France). We are grateful to Laurent David (Inserm 1064, Nantes) and Bernard Jost (GenomEast platform, IGBMC, Strasbourg, France). We thank Justine Poirot for help in single cell analyses. We acknowledge the contribution of AniRA lentivectors production facility from the CELPHEDIA Infrastructure and SFR Biosciences (UAR3444/CNRS, US8/Inserm, ENS de Lyon, UCBL), especially Gisèle Froment, Didier Nègre and Caroline Costa. We also thank Sophie Ezine and Bela Papp for critical discussions. This work was supported by the Agence de la Biomédecine, Agence National de la Recherche (ANR EpiDev), the Institut National Du Cancer (InCA B-REC), the Fondation Ramsay Générale de Santé and by the Inserm HuDeCA network.

AUTHOR CONTRIBUTIONS

Conceptualization: BC, KAH.
Methodology: EN, SL, BE, MD, SD, GPA, FC, AL.
Investigation: KAH, EC, SL, SK, EV, KC, ZK.
Funding acquisition: BC, DG, MG, AC.
Writing – original draft: BC, KAH, EAM, VA, ZK, AC, FC.
Supervision: BC.

DECLARATION OF INTERESTS

The authors have no conflict of interest.

Received: February 27, 2023
Revised: August 24, 2023
Accepted: September 7, 2023
Published: September 9, 2023

REFERENCES

1. Laurenti, E., and Göttgens, B. (2018). From haematopoietic stem cells to complex differentiation landscapes. Nature *553*, 418–426. https://doi.org/10.1038/nature25022.
2. Pronk, C.J.H., Rossi, D.J., Månsson, R., Attema, J.L., Norddahl, G.L., Chan, C.K.F., Sigvardsson, M., Weissman, I.L., and Bryder, D. (2007). Elucidation of the phenotypic, functional, and molecular topography of a myeloerythroid progenitor cell hierarchy. Cell Stem Cell *1*, 428–442. https://doi.org/10.1016/j.stem.2007.07.005.
3. Sanjuan-Pla, A., Macaulay, I.C., Jensen, C.T., Woll, P.S., Luis, T.C., Mead, A., Moore, S., Carella, C., Matsuoka, S., Bouriez Jones, T., et al. (2013). Platelet-biased stem cells reside at the apex of the haematopoietic stem-cell hierarchy. Nature *502*, 232–236. https://doi.org/10.1038/nature12495.
4. Yamamoto, R., Morita, Y., Ooehara, J., Hamanaka, S., Onodera, M., Rudolph, K.L., Ema, H., and Nakauchi, H. (2013). Clonal analysis unveils self-renewing lineage-restricted progenitors generated directly from hematopoietic stem cells. Cell *154*, 1112–1126. https://doi.org/10.1016/j.cell.2013.08.007.
5. Mossadegh-Keller, N., Sarrazin, S., Kandalla, P.K., Espinosa, L., Stanley, E.R., Nutt, S.L., Moore, J., and Sieweke, M.H. (2013). M-CSF instructs myeloid lineage fate in single haematopoietic stem cells. Nature *497*, 239–243. https://doi.org/10.1038/nature12026.
6. Rieger, M.A., Hoppe, P.S., Smejkal, B.M., Eitelhuber, A.C., and Schroeder, T. (2009). Hematopoietic cytokines can instruct lineage choice. Science *325*, 217–218. https://doi.org/10.1126/science.1171461.
7. Benz, C., Copley, M.R., Kent, D.G., Wohrer, S., Cortes, A., Aghaeepour, N., Ma, E., Mader, H., Rowe, K., Day, C., et al. (2012). Hematopoietic stem cell subtypes expand differentially during development and display distinct lymphopoietic programs. Cell Stem Cell *10*, 273–283. https://doi.org/10.1016/j.stem.2012.02.007.
8. Rodriguez-Fraticelli, A.E., Wolock, S.L., Weinreb, C.S., Panero, R., Patel, S.H., Jankovic, M., Sun, J., Calogero, R.A., Klein, A.M., and Camargo, F.D. (2018). Clonal analysis of lineage fate in native haematopoiesis. Nature *553*, 212–216. https://doi.org/10.1038/nature25168.
9. Kim, S., Kim, N., Presson, A.P., Metzger, M.E., Bonifacino, A.C., Sehl, M., Chow, S.A., Crooks, G.M., Dunbar, C.E., An, D.S., et al. (2014). Dynamics of HSPC repopulation in nonhuman primates revealed by a decade-long clonal-tracking study. Cell Stem Cell *14*, 473–485. https://doi.org/10.1016/j.stem.2013.12.012.
10. Biasco, L., Pellin, D., Scala, S., Dionisio, F., Basso-Ricci, L., Leonardelli, L., Scaramuzza, S., Baricordi, C., Ferrua, F., Cicalese, M.P., et al. (2016). In Vivo Tracking of Human Hematopoiesis Reveals Patterns of Clonal Dynamics during Early and Steady-State Reconstitution Phases. Cell Stem Cell *19*, 107–119. https://doi.org/10.1016/j.stem.2016.04.016.
11. Six, E., Guilloux, A., Denis, A., Lecoules, A., Magnani, A., Vilette, R., Male, F., Cagnard, N., Delville, M., Magrin, E., et al. (2020). Clonal tracking in gene therapy patients reveals a diversity of human hematopoietic differentiation programs. Blood *135*, 1219–1231. https://doi.org/10.1182/blood.2019002350.
12. Weinreb, C., Rodriguez-Fraticelli, A., Camargo, F.D., and Klein, A.M. (2020). Lineage tracing on transcriptional landscapes links state to fate during differentiation. Science *367*, eaaw3381. https://doi.org/10.1126/science.aaw3381.
13. Park, B.G., Park, C.J., Jang, S., Chi, H.S., Kim, D.Y., Lee, J.H., Lee, J.H., and Lee, K.H. (2015). Reconstitution of lymphocyte subpopulations after hematopoietic stem cell transplantation: comparison of hematologic malignancies and donor types in event-free patients. Leuk. Res. *39*, 1334–1341. https://doi.org/10.1016/j.leukres.2015.09.010.
14. Upadhaya, S., Sawai, C.M., Papalexi, E., Rashidfarrokhi, A., Jang, G., Chattopadhyay, P., Satija, R., and Reizis, B. (2018). Kinetics of adult hematopoietic stem cell differentiation in vivo. J. Exp. Med. *215*, 2815–2832. https://doi.org/10.1084/jem.20180136.
15. Adolfsson, J., Månsson, R., Buza-Vidas, N., Hultquist, A., Liuba, K., Jensen, C.T., Bryder, D., Yang, L., Borge, O.J., Thoren, L.A.M., et al. (2005). Identification of Flt3+ lympho-myeloid stem cells lacking erythro-megakaryocytic potential a revised road map for adult blood lineage commitment. Cell *121*, 295–306. https://doi.org/10.1016/j.cell.2005.02.013.
16. Sitnicka, E., Bryder, D., Theilgaard-Mönch, K., Buza-Vidas, N., Adolfsson, J., and Jacobsen, S.E.W. (2002). Key role of flt3 ligand in regulation of the common lymphoid progenitor but not in maintenance of the hematopoietic stem cell pool. Immunity *17*, 463–472. https://doi.org/10.1016/s1074-7613(02)00419-3.
17. Amann-Zalcenstein, D., Tian, L., Schreuder, J., Tomei, S., Lin, D.S., Fairfax, K.A., Bolden, J.E., McKenzie, M.D., Jarratt, A., Hilton, A., et al. (2020). A new lymphoid-primed progenitor marked by Dach1 downregulation identified with single cell multi-omics. Nat. Immunol. *21*, 1574–1584. https://doi.org/10.1038/s41590-020-0799-x.
18. Igarashi, H., Gregory, S.C., Yokota, T., Sakaguchi, N., and Kincade, P.W. (2002). Transcription from the RAG1 locus marks the earliest lymphocyte progenitors in bone marrow. Immunity *17*, 117–130.
19. Klein, F., Roux, J., Cvijetic, G., Rodrigues, P.F., von Muenchow, L., Lubin, R., Pelczar, P., Yona, S., Tsapogas, P., and Tussiwand, R. (2022). Dntt expression reveals developmental hierarchy and lineage specification of hematopoietic progenitors. Nat. Immunol. *23*, 505–517. https://doi.org/10.1038/s41590-022-01167-5.
20. Cumano, A., Berthault, C., Ramond, C., Petit, M., Golub, R., Bandeira, A., and Pereira, P. (2019). New Molecular Insights into Immune Cell Development. Annu. Rev. Immunol. *37*, 497–519. https://doi.org/10.1146/annurev-immunol-042718-041319.
21. Canque, B., Camus, S., Dalloul, A., Kahn, E., Yagello, M., Dezutter-Dambuyant, C., Schmitt, D., Schmitt, C., and Gluckman, J.C. (2000). Characterization of dendritic cell differentiation pathways from cord blood CD34(+)CD7(+)CD45RA(+) hematopoietic progenitor cells. Blood *96*, 3748–3756.
22. Fritsch, G., Buchinger, P., Printz, D., Fink, F.M., Mann, G., Peters, C., Wagner, T., Adler, A., and Gadner, H. (1993). Rapid discrimination of early CD34+ myeloid progenitors using CD45-RA analysis. Blood *81*, 2301–2309.
23. Doulatov, S., Notta, F., Eppert, K., Nguyen, L.T., Ohashi, P.S., and Dick, J.E. (2010). Revised map of the human progenitor hierarchy shows the origin of macrophages and dendritic cells in early lymphoid development. Nat. Immunol. *11*, 585–593. https://doi.org/10.1038/ni.1889.
24. Haddad, R., Guardiola, P., Izac, B., Thibault, C., Radich, J., Delezoide, A.L., Baillou, C., Lemoine, F.M., Gluckman, J.C., Pflumio, F., and Canque, B. (2004). Molecular characterization of early human T/NK and B-lymphoid progenitor cells in umbilical cord blood. Blood *104*, 3918–3926. https://doi.org/10.1182/blood-2004-05-1845; 2004-05-1845.
25. Hao, Q.L., Zhu, J., Price, M.A., Payne, K.J., Barsky, L.W., and Crooks, G.M. (2001). Identification of a novel, human multilymphoid progenitor in cord blood. Blood *97*, 3683–3690.
26. Hoebeke, I., De Smedt, M., Stolz, F., Pike-Overzet, K., Staal, F.J.T., Plum, J., and Leclercq, G. (2007). T-B- and NK-lymphoid, but not myeloid cells arise from human CD34(+)CD38(-)CD7(+) common lymphoid progenitors expressing lymphoid-specific genes. Leukemia *21*, 311–319. https://doi.org/10.1038/sj.leu.2404488.
27. Galy, A., Travis, M., Cen, D., and Chen, B. (1995). Human T, B, natural killer, and dendritic cells arise from a common bone marrow progenitor cell subset. Immunity *3*, 459–473.
28. Karamitros, D., Stoilova, B., Aboukhalil, Z., Hamey, F., Reinisch, A., Samitsch, M., Quek, L., Otto, G., Repapi, E., Doondeea, J., et al. (2018). Single-cell analysis reveals the continuum of human lympho-myeloid progenitor cells. Nat. Immunol. *19*, 85–97. https://doi.org/10.1038/s41590-017-0001-2.
29. Haddad, R., Guimiot, F., Six, E., Jourquin, F., Setterblad, N., Kahn, E., Yagello, M., Schiffer, C., Andre-Schmutz, I., Cavazzana-Calvo, M., et al. (2006). Dynamics of thymus-colonizing cells during human development. Immunity *24*, 217–230. https://doi.org/10.1016/j.immuni.2006.01.008.
30. Keita, S., Diop, S., Lekiashvili, S., Chabaane, E., Nelson, E., Strullu, M., Arfeuille, C., Guimiot, F., Domet, T., Duchez, S., et al. (2023). Distinct subsets of multi-lymphoid progenitors support ontogeny-related changes in human lymphopoiesis. Cell Rep. *42*, 112618. https://doi.org/10.1016/j.celrep.2023.112618.
31. Jardine, L., Webb, S., Goh, I., Quiroga Londoño, M., Reynolds, G., Mather, M., Olabi, B., Stephenson, E., Botting, R.A., Horsfall, D., et al. (2021). Blood and immune development in human fetal bone marrow and Down syndrome. Nature *598*, 327–331. https://doi.org/10.1038/s41586-021-03929-x.
32. Suo, C., Dann, E., Goh, I., Jardine, L., Kleshchevnikov, V., Park, J.E., Botting, R.A., Stephenson, E., Engelbert, J., Tuong, Z.K., et al. (2022). Mapping the developing human immune system across organs. Science *376*, eabo0510. https://doi.org/10.1126/science.abo0510.
33. Ranzoni, A.M., Tangherloni, A., Berest, I., Riva, S.G., Myers, B., Strzelecka, P.M., Xu, J., Panada, E., Mohorianu, I., Zaugg, J.B., and Cvejic, A. (2021). Integrative Single-Cell RNA-Seq and ATAC-Seq Analysis of Human

Developmental Hematopoiesis. Cell Stem Cell *28*, 472–487.e7. https://doi.org/10.1016/j.stem.2020.11.015.

34. Roy, A., Wang, G., Iskander, D., O'Byrne, S., Elliott, N., O'Sullivan, J., Buck, G., Heuston, E.F., Wen, W.X., Meira, A.R., et al. (2021). Transitions in lineage specification and gene regulatory networks in hematopoietic stem/progenitor cells over human development. Cell Rep. *36*, 109698. https://doi.org/10.1016/j.celrep.2021.109698.
35. Parietti, V., Nelson, E., Telliam, G., Le Noir, S., Pla, M., Delord, M., Vanneaux, V., Mohtashami, M., Macintyre, E.A., Gluckman, J.C., et al. (2012). Dynamics of human prothymocytes and xenogeneic thymopoiesis in hematopoietic stem cell-engrafted nonobese diabetic-SCID/IL-2rgammanull mice. J. Immunol. *189*, 1648–1660. https://doi.org/10.4049/jimmunol.1201251.
36. Alhaj Hussen, K., Vu Manh, T.P., Guimiot, F., Nelson, E., Chabaane, E., Delord, M., Barbier, M., Berthault, C., Dulphy, N., Alberdi, A.J., et al. (2017). Molecular and Functional Characterization of Lymphoid Progenitor Subsets Reveals a Bipartite Architecture of Human Lymphopoiesis. Immunity *47*, 680–696.e8. https://doi.org/10.1016/j.immuni.2017.09.009.
37. Lin, C.C., Yao, C.Y., Hsu, Y.C., Hou, H.A., Yuan, C.T., Li, Y.H., Kao, C.J., Chuang, P.H., Chiu, Y.C., Chen, Y., et al. (2020). Knock-out of Hopx disrupts stemness and quiescence of hematopoietic stem cells in mice. Oncogene *39*, 5112–5123. https://doi.org/10.1038/s41388-020-1340-2.
38. Vitali, C., Bassani, C., Chiodoni, C., Fellini, E., Guarnotta, C., Miotti, S., Sangaletti, S., Fuligni, F., De Cecco, L., Piccaluga, P.P., et al. (2015). SOCS2 Controls Proliferation and Stemness of Hematopoietic Cells under Stress Conditions and Its Deregulation Marks Unfavorable Acute Leukemias. Cancer Res. *75*, 2387–2399. https://doi.org/10.1158/0008-5472.CAN-14-3625.
39. Mann, Z., Sengar, M., Verma, Y.K., Rajalingam, R., and Raghav, P.K. (2022). Hematopoietic Stem Cell Factors: Their Functional Role in Self-Renewal and Clinical Aspects. Front. Cell Dev. Biol. *10*, 664261. https://doi.org/10.3389/fcell.2022.664261.
40. de Laval, B., Pawlikowska, P., Petit-Cocault, L., Bilhou-Nabera, C., Aubin-Houzelstein, G., Souyri, M., Pouzoulet, F., Gaudry, M., and Porteu, F. (2013). Thrombopoietin-increased DNA-PK-dependent DNA repair limits hematopoietic stem and progenitor cell mutagenesis in response to DNA damage. Cell Stem Cell *12*, 37–48. https://doi.org/10.1016/j.stem.2012.10.012.
41. Street, K., Risso, D., Fletcher, R.B., Das, D., Ngai, J., Yosef, N., Purdom, E., and Dudoit, S. (2018). Slingshot: cell lineage and pseudotime inference for single-cell transcriptomics. BMC Genom. *19*, 477. https://doi.org/10.1186/s12864-018-4772-0.
42. Sitnicka, E., Brakebusch, C., Martensson, I.L., Svensson, M., Agace, W.W., Sigvardsson, M., Buza-Vidas, N., Bryder, D., Cilio, C.M., Ahlenius, H., et al. (2003). Complementary signaling through flt3 and interleukin-7 receptor alpha is indispensable for fetal and adult B cell genesis. J. Exp. Med. *198*, 1495–1506. https://doi.org/10.1084/jem.20031152.
43. Sitnicka, E., Buza-Vidas, N., Ahlenius, H., Cilio, C.M., Gekas, C., Nygren, J.M., Månsson, R., Cheng, M., Jensen, C.T., Svensson, M., et al. (2007). Critical role of FLT3 ligand in IL-7 receptor independent T lymphopoiesis and regulation of lymphoid-primed multipotent progenitors. Blood *110*, 2955–2964. https://doi.org/10.1182/blood-2006-10-054726.
44. Månsson, R., Hultquist, A., Luc, S., Yang, L., Anderson, K., Kharazi, S., Al-Hashmi, S., Liuba, K., Thorén, L., Adolfsson, J., et al. (2007). Molecular evidence for hierarchical transcriptional lineage priming in fetal and adult stem cells and multipotent progenitors. Immunity *26*, 407–419. https://doi.org/10.1016/j.immuni.2007.02.013.
45. Allman, D., Sambandam, A., Kim, S., Miller, J.P., Pagan, A., Well, D., Meraz, A., and Bhandoola, A. (2003). Thymopoiesis independent of common lymphoid progenitors. Nat. Immunol. *4*, 168–174. https://doi.org/10.1038/ni878.
46. Berthault, C., Ramond, C., Burlen-Defranoux, O., Soubigou, G., Chea, S., Golub, R., Pereira, P., Vieira, P., and Cumano, A. (2017). Asynchronous lineage priming determines commitment to T cell and B cell lineages in fetal liver. Nat. Immunol. *18*, 1139–1149. https://doi.org/10.1038/ni.3820.
47. Kawamoto, H., Ikawa, T., Ohmura, K., Fujimoto, S., and Katsura, Y. (2000). T cell progenitors emerge earlier than B cell progenitors in the murine fetal liver. Immunity *12*, 441–450.
48. Paul, F., Arkin, Y., Giladi, A., Jaitin, D.A., Kenigsberg, E., Keren-Shaul, H., Winter, D., Lara-Astiaso, D., Gury, M., Weiner, A., et al. (2016). Transcriptional Heterogeneity and Lineage Commitment in Myeloid Progenitors. Cell *164*, 325. https://doi.org/10.1016/j.cell.2015.12.046.
49. Velten, L., Haas, S.F., Raffel, S., Blaszkiewicz, S., Islam, S., Hennig, B.P., Hirche, C., Lutz, C., Buss, E.C., Nowak, D., et al. (2017). Human haematopoietic stem cell lineage commitment is a continuous process. Nat. Cell Biol. *19*, 271–281. https://doi.org/10.1038/ncb3493.
50. Cacchiarelli, D., Trapnell, C., Ziller, M.J., Soumillon, M., Cesana, M., Karnik, R., Donaghey, J., Smith, Z.D., Ratanasirintrawoot, S., Zhang, X., et al. (2015). Integrative Analyses of Human Reprogramming Reveal Dynamic Nature of Induced Pluripotency. Cell *162*, 412–424. https://doi.org/10.1016/j.cell.2015.06.016.
51. Thielecke, L., Aranyossy, T., Dahl, A., Tiwari, R., Roeder, I., Geiger, H., Fehse, B., Glauche, I., and Cornils, K. (2017). Limitations and challenges of genetic barcode quantification. Sci. Rep. *7*, 43249. https://doi.org/10.1038/srep43249.
52. Thielecke, L., Cornils, K., and Glauche, I. (2020). genBaRcode: a comprehensive R-package for genetic barcode analysis. Bioinformatics *36*, 2189–2194. https://doi.org/10.1093/bioinformatics/btz872.
53. Giacosa, S., Pillet, C., Séraudie, I., Guyon, L., Wallez, Y., Roelants, C., Battail, C., Evrard, B., Chalmel, F., Barette, C., et al. (2021). Cooperative Blockade of CK2 and ATM Kinases Drives Apoptosis in VHL-Deficient Renal Carcinoma Cells through ROS Overproduction. Cancers *13*, 576. https://doi.org/10.3390/cancers13030576.
54. Love, M.I., Huber, W., and Anders, S. (2014). Moderated estimation of fold change and dispersion for RNA-seq data with DESeq2. Genome Biol. *15*, 550. https://doi.org/10.1186/s13059-014-0550-8.
55. Chalmel, F., and Primig, M. (2008). The Annotation, Mapping, Expression and Network (AMEN) suite of tools for molecular systems biology. BMC Bioinf. *9*, 86. https://doi.org/10.1186/1471-2105-9-86.
56. Ritchie, J.B., Tovar, D.A., and Carlson, T.A. (2015). Emerging Object Representations in the Visual System Predict Reaction Times for Categorization. PLoS Comput. Biol. *11*, e1004316. https://doi.org/10.1371/journal.pcbi.1004316.
57. Smyth, G.K. (2004). Linear models and empirical bayes methods for assessing differential expression in microarray experiments. Stat. Appl. Genet. Mol. Biol. *3*, Article3. https://doi.org/10.2202/1544-6115.1027.
58. Ritchie, M.E., Phipson, B., Wu, D., Hu, Y., Law, C.W., Shi, W., and Smyth, G.K. (2015). limma powers differential expression analyses for RNA-sequencing and microarray studies. Nucleic Acids Res. *43*, e47. https://doi.org/10.1093/nar/gkv007.
59. Wettenhall, J.M., and Smyth, G.K. (2004). limmaGUI: a graphical user interface for linear modeling of microarray data. Bioinformatics *20*, 3705–3706. https://doi.org/10.1093/bioinformatics/bth449.
60. Van den Berge, K., Roux de Bézieux, H., Street, K., Saelens, W., Cannoodt, R., Saeys, Y., Dudoit, S., and Clement, L. (2020). Trajectory-based differential expression analysis for single-cell sequencing data. Nat. Commun. *11*, 1201. https://doi.org/10.1038/s41467-020-14766-3.

STAR★METHODS

KEY RESOURCES TABLE

REAGENT or RESOURCE	SOURCE	IDENTIFIER
Antibodies		
anti-human CD45 AF700	BioLegend	Cat# 304011304024; RRID:AB_493761
anti-human CD34 Pacific Blue	BioLegend	Cat# 343512; RRID:AB_1877197
anti-human CD7 FITC	Beckman Coulter	Cat# A07755
anti-human CD38 PerCPCy5.5	BioLegend	Cat# 303522; RRID:AB_893314
anti-human CD33 PE-CF594	BD Biosciences	Cat#
anti-human CD115 APC	BioLegend	Cat# 347306; RRID:AB_2562441
anti-human CD71 PE	BD Biosciences	Cat# 555537; RRID:AB_395921
anti-human ITGB7 PECy7	ThermoFisher	Cat# 25-5867-42; RRID:AB_2573481
anti-human CD3 PE-CF594	BD Biosciences	Cat# 562310; RRID:AB_11153505
anti-human CD14 PE-CF594	BD Biosciences	Cat# 562335; RRID:AB_11153663
anti-human CD19 PE-DAZZLE	BioLegend	Cat# 302252; RRID:AB_2563560
anti-human CD24 PE-CF594	BD Biosciences	Cat# 562405; RRID:AB_11153321
anti-human CD56 PE-CF594	BD Biosciences	Cat# 562289; RRID:AB_11152080
anti-human CD45RA BV711	BioLegend	Cat# 304138; RRID:AB_2563815
anti-human CD116 APC-vio770	Miltenyi	Cat# 130-100-992; RRID:AB_2654571
anti-human CD127 PECy5	BioLegend	Cat# 351324; RRID:AB_10915554
anti-human CD117 BV605	BioLegend	Cat# 313218; RRID:AB_2562025
anti-human CD10 BV650	BD Biosciences	Cat# 563734; RRID:AB_2738393
anti-human CD123 BV786	BD Biosciences	Cat# 564196; RRID:AB_2738662
anti-human CD45RA PE	BD Biosciences	Cat# 555489; RRID:AB_395880
anti-human CD19 BV711	BD Biosciences	Cat# 302245; RRID:AB_2562062
anti-human CD7 PE-CF594	BD Biosciences	Cat# 562541; RRID:AB_2737642
anti-human CD15 BV605	BD Biosciences	Cat# 562978562979; RRID:AB_2744292
Zombie Violet	BioLegend	Cat# 423113
Biological samples		
Umbilical cord blood	Unité de Thérapie Cellulaire of Hôpital Saint-Louis (Paris)	N/A
Chemicals, peptides, and recombinant proteins		
BIT 9500	StemCell Technologies	Cat#09500
Bovine serum albumin	Eurobio	Cat#GAUBSA0165
Dimethyl sulfoxide	Sigma Aldrich	Cat#D4540
Fc receptor-binding inhibitor	eBioscience	Cat#16-9161-73
Fetal calf serum	Life Technologies	Cat#10270106
Ficoll-Hypaque	Pancoll, PAN Biotech GmbH	Cat#P04-60500
Human FLT3L, premium grade	Miltenyi Biotech	Cat#130-096-479
Human G-CSF, premium grade	Miltenyi Biotech	Cat#130-093-861
Human TSLP, research grade	Miltenyi Biotech	Cat#130-106-270
Human GM-CSF, premium grade	Miltenyi Biotech	Cat#130-093-866
Human IL-2 IS, premium grade	Miltenyi Biotech	Cat#130-097-744
Human IL-3, premium grade	Miltenyi Biotech	Cat#130-095-069
Human IL-7, premium grade	Miltenyi Biotech	Cat#130-095-363

(*Continued on next page*)

Continued

REAGENT or RESOURCE	SOURCE	IDENTIFIER
Human IL-15, premium grade	Miltenyi Biotech	Cat#130-095-765
Human M-CSF, premium grade	Miltenyi Biotech	Cat#130-096-492
Human SCF, premium grade	Miltenyi Biotech	Cat#130-096-695
Human TPO, premium grade	Miltenyi Biotech	Cat#130-095-752
Human IL-21, premium grade	Miltenyi Biotech	Cat#130-095-768
Human IL-12, premium grade	Miltenyi Biotech	Cat#130-096-704
Human IL-6, premium grade	Miltenyi Biotech	Cat#130-095-365
Human IL-27, premium grade	Miltenyi Biotech	Cat#130-108-961
Human IL-10, research grade	Miltenyi Biotech	Cat#130-093-948
Human TNFa, research grade	Miltenyi Biotech	Cat#130-094-015
Human TGFb, premium grade	Miltenyi Biotech	Cat#130-108-971
Human IL-9, research grade	Miltenyi Biotech	Cat#130-093-946
Human IL-13, research grade	Miltenyi Biotech	Cat#130-112-409
Human IL-33, research grade	Miltenyi Biotech	Cat#130-109-378
RNase-free DNase I	Roche	Cat#1284932
SUPERase-In RNase Inhibitor	Ambion	Cat#AM2694
2-mercaptoethanol	Life Technologies	Cat#31350010
Maxima H Minus Reverse Transcriptase	Thermo Fisher	Cat# EP0752
Exonuclease	New EnglandBiolabs	Cat# M0293L
Critical commercial assays		
CD34 Microbead kit	Miltenyi Biotech	Cat#130-046-702
Mouse Cell Depletion Kit	Miltenyi Biotech	Cat#130-104-694
CellsDirect one-step qRT-PCR kit	Invitrogen	Cat#11753500
DNA Clean and Concentrtor TM-5	ZYMO RESEARCH	Cat#D4013
Advantage 2 PCR Kit	Clontech	Cat#639206
Agencourt AMPure XP	Beckman Coulter	Cat#A63880
Nextera DNA Flex Library Prep	Illumina	Cat#20018704
Single Cell 3′ Kit v3.1	10X Genomics	Cat#PN-1000128
Deposited data		
Raw and pre-processed data	This paper	GSE215296 GSE214950
Experimental models: Cell lines		
Mouse: OP9	A. Cumano, Institut Pasteur	N/A
Mouse: OP9-DL4	A. Cumano, Institut Pasteur	N/A
Experimental models: Organisms/strains		
Mouse: NOD.Cg-PrkdcscidIL2RGtm1wjl/SzJ (005557)	Jackson Laboratory	N/A
Oligonucleotides		
Nextera™ DNA CD Indexes	illumina	20018708
Taqman probes	Life Technologies	See Table S3
Software and algorithms		
FlowJo software (10.7)	TreeStar Inc.	N/A
Prism 9	Prism-Graphpad	www.graphpad.com
R	N/A	https://www.r-project.org/

(*Continued on next page*)

Continued

REAGENT or RESOURCE	SOURCE	IDENTIFIER
Biomark qPCR analysis software	Fluidigm	N/A
genBaRcode package	N/A	https://cran.r-project.org/web/packages/genBaRcode

RESOURCE AVAILABILITY

Lead contact

Further information and requests for resources should be directed to and will be fulfilled by the lead contact, Bruno Canque (bruno.canque@ephe.psl.eu).

Materials availability

This study did not generate new unique reagents.

Data and code availability

- RNA-seq data have been deposited at GEO and are publicly available. Accession numbers are listed in the key resources table.
- This paper does not report original code.
- Any additional information required to reanalyze the data reported in this paper is available from the lead contact upon request.

EXPERIMENTAL MODELS AND STUDY PARTICIPANT DETAILS

Human sample collection

Umbilical cord blood (UCB) was provided by the Unité de Thérapie Cellulaire of Hôpital Saint-Louis (Paris). No limitations were placed on analyzed samples in terms of donor ancestry, race, or ethnicity.

Mice

NOD.Cg-Prkdc^{scid}IL2RG^{tm1wjl}/SzJ (005557) mice known as NOD scid gamma (NSG) mice (Jackson Laboratory, Bar Harbor, MI) were housed in the pathogen-free animal facility of Institut de Recherche Saint Louis (Paris). Female NSG mice were xenografted at 2 months of age. The Ethical Committee at Paris Nord University approved all performed experiments.

METHODS DETAILS

Processing of human cord blood and cell separation

Blood cells were separated by Ficoll-Hypaque centrifugation (Pancoll, PAN Biotech GmbH) before processing for flow cytometry, cell sorting or CD34$^+$ HSPC isolation. Human CD34$^+$ cells were isolated from umbilical cord bloods pooled from 1 to 3 donors with the CD34 Microbead kit (Miltenyi Biotech; purity >90%), frozen in heat-inactivated fetal calf serum (FCS) supplemented with 10% DMSO and stored in liquid nitrogen until use. After thawing, CD34$^+$ HPCs were UCBs were labeled with a dedicated antibody cocktail before sorting of CD34^{hi}CD45RA$^-$CD38$^{lo/-}$Lin$^-$ HSPCs (Lin: CD3, CD10, CD14, CD19, CD24, CD56, CD71, CD115, CD116, CD123; see also Figure S1A for the gating procedure).

Xeno-transplantations

Xeno-transplantations were performed essentially as described.[36] NOD scid gamma (NSG) mice (Jackson Laboratory, Bar Harbor, MI) housed in the pathogen-free animal facility of Institut de Recherche Saint Louis (Paris) were irradiated (2.25 Gy) 24-h before injection of FACS sorted CD34$^+$CD45RA$^-$Lin$^-$ HSPCs (2 × 10^5 cells/mouse) in the caudal vein. Recipient NSG mice were sacrificed between week-1 and week-5 after grafting. The Ethical Committee at Paris Nord University approved all performed experiments.

Flow cytometry and cell sorting

Single-cell suspensions recovered from the femurs and tibias of xenografted mice were filtered through a cell strainer (70 μm; BD biosciences) and depleted in mouse cells using the Mouse Cell Depletion Kit (Miltenyi) before being processed for Flow Cytometry. Human single-cell suspensions were incubated with human Fc receptor-binding inhibitor (Fc Block, eBioscience) before surface staining with anti-human monoclonal antibodies (mAbs). Fluorescence minus one (FMO) controls with control isotype antibodies were used to define positive signals for flow cytometry or cell sorting. Dead cells were excluded with the Zombie Violet Fixable Viability Kit (Biolegend). For labeling, cells were re-suspended in PBS, 2% FCS (1–5 × 10^7 cells/500 μL) and incubated with the following mAbs: CD45 AF700 (Biolegend, clone HI30), CD34 PB (Biolegend, clone 581), CD7 FITC (Beckman Coulter, clone 8H8.1), CD38 PerCPCy5.5 (Biolegend, clone HIT2), CD123 BV785 (BD Bioscience, clone 7G3), CD115 APC (Biolegend, clone 9-4D2-1E4), CD45RA PE (BD Bioscience, clone HIT100), ITGB7 PC7 (eBioscience, clone FIB504),

CD33 PE-CF594 (BD Bioscience, clone WM53), CD19 BV711 (BD bioscience, clone HIB19), CD116 APC-vio770 (Miltenyi, clone REA211), CD127 PC5 (Biolegend, clone A019D5), CD117 BV605 (Biolegend, clone 104D2), CD10 BV650 (BD bioscience, clone HI10a), also CD7 PE-CF594 (BD Bioscience, clone M-T701). Flow cytometry and cell sorting were performed with a BD Fortessa Analyzer or a BD FACSAria III sorter (BD Biosciences; (purity ≥95%). Flow cytometry analyses were performed using the FlowJo software (Version 10.7).

For investigating the effect of conservative cell division on the lymphoid differentiation potential, neonatal HSC or LMDPs sorted from the UCB were labeled with proliferation-dependent dye carboxyfluorescein diacetate succinimidyl ester (CFSE) using the Vybrant CFDA SE Cell Tracer Kit (Life Technologies) prior injection to irradiated NSG mice (2×10^5 cells/mouse). Mice engrafted with the CFSE-labeled cells were sacrificed 8 days later before huCD45$^+$ BM cells were labeled with the same antibody cocktail as above except for the CD7 antibody (CD7 PE-CF594; BD Bioscience, clone M-T701).

Cell cultures and analysis

For multi-lineage diversification assays under bulk conditions (100 cell/well), OP9 or OP9-DL4 stromal cells were seeded in Opti-MEM-Glutamax supplemented with 2.5% FCS, 7.5% BIT 9500 (StemCell Technologies), 1% penicillin-streptomycin and 1/1000 β-mercapto-ethanol (Life Technologies) in 96-well U-bottom plates 24 h prior to co-culture with the indicated combinations of growth/differentiation factors (10 ng/mL each; all from Miltenyi Biotec). CD34$^+$ HSPCs isolated from the BM of xenografted mice sacrificed between weeks 1–5 after grafting were directly seeded by FACS in the 96-well plates and cultured for 7 or 14 days before quantification of lineage outputs. Clonal diversification assays were conducted for 14 days under the same condition, except that cultures were supplemented with SCF, TPO and GM-CSF (10 ng/mL each).

For assessment of lineage output, in vitro-differentiated cells were labeled with the following antibodies: CD45 AF700 (Biolegend, clone HI30), CD34 PB (Biolegend, clone 581), CD7 FITC (Beckman Coulter, clone 8H8.1), CD123 BV786 (BD Bioscience, clone 7G3), CD115 APC (Biolegend, clone 9-4D2-1E4), CD45RA PE (BD Bioscience, clone HIT100), ITGB7 PC7 (eBioscience, clone FIB504), CD24 PE-CF594 (BD Bioscience, clone ML5), CD19 BV711 (BD bioscience, clone HIB19), CD116 APC-vio770 (Miltenyi, clone REA211), CD127 PC5 (Biolegend, clone A019D5), CD15 BV605 (BD Bioscience, clone HI10a), CD10 BV650 (BD bioscience, clone HI98). Flow cytometry analyses were performed with a BD Fortessa Analyzer and the FlowJo software.

Transcriptional profiling by multiplex PCR

Gene expression analyses were performed with the Fluidigm 96.96 Dynamic Array IFC and TaqMan Gene Expression Assays (Life Technologies). The indicated cell subsets were sorted by 50 cell pools directly into 96-well PCR plate containing 2.5 mL TaqMan specific gene assay mix (Applied Biosystems), 5 mL of CellsDirect 2x Reaction mix, 0.2 mL SuperScript TM III RT/PlatinumR Taq Mix (Invitrogen, CellsDirect one-step qRT-PCR kit), 1.2 mL TE buffer, and 0.1 mL SUPERase-In RNase Inhibitor (Ambion). Reverse transcription was performed for 15 min at 50°C followed by 2 min at 95°C for RT inactivation before cDNAs were pre-amplified for 21 cycles at 95°C for 15 s and 60°C for 4 min. Pre-amplified products were diluted 1:5 in TE buffer and analyzed on a Biomark system (Fluidigm) with the following PCR cycling condition: 95°C for 10 min and 40 cycles at 95°C for 15 s and 60°C for 60 s. Data were analyzed using the Biomark qPCR Analysis software (Fluidigm). For quantification of gene expression, data were analyzed by the DDCt method. Results were normalized relative to HPRT expression and expressed as mean expression level of ≥6 biological replicates. Hierarchical clustering was performed on standardized means of gene expression levels based on Euclidean distance using the ''pheatmap'' R package. A complete list of the TaqMan primers is provided as Table S2.

Gene expression profiling by mini-RNA-seq

The protocol used for mini-RNAseq was adapted from the method developed by Soumillon et al.[50] For each cell population batches of 100 cells (2–10 replicates) were sorted by FACS in 96-well V-bottom plate wells containing 2 µL of lysis buffer (Ultra-pure Water, 10% Triton X-100, RNasinPlus 40U/ul; Promega). After evaporation of the lysis buffer at 95°C for 3 min, first strand cDNA synthesis was performed using the Maxima H Minus Reverse Transcriptase (Thermo Fisher), E3V6NEXT primers (specific primer for each well) and Template Switching Primer: E5V6NEXT. Resulting cDNAs were pooled and purified by the DNA Clean and Concentrator TM-5 kit (Zymo research) and treated with Exonuclease I (New England Biolabs) before amplification using the Advantage 2 PCR kit (Clontech) and the SINGV6 primer (95°C for 1 min, 15 cycles at 95°C for 15 s, 65°C for 30 s, 68°C for 6 min, and 72°C for 10 min). PCR products were purified by Agencourt AMPure XP (Beckman Coulter). Libraries were prepared using the Illumina DNA Prep kit (Illumina) according to the manufacturer's guidelines and sequenced on a HiSeq 4000 (Illumina) at the Genome East Platform of the IGBMC (Strasbourg, France). Image analysis and base calling were performed using RTA 2.7.7 and bcl2fastq 2.17.1.14 software. Adapter dimer reads were removed using Dimer Remover (https://sourceforge.net/projects/dimerremover/).

Single cell-RNA-seq

For the droplet encapsulation $2{,}5 \times 10^4$ live, single, HSC/MPP (CD45RA$^{-/int}$), LMDP (CD45RA^{hi}ITGB7$^-$), CD127$^-$ (ITGB7$^{lo/+}$) or CD127$^+$ (ITGB7$^{-/+}$) cells isolated by FACS from the BM of NSG-UCB mice at week-3 after grafting were loaded onto each channel of a Chromium chip before encapsulation on the Chromium Controller (10x Genomics). Single-cell sequencing libraries were generated using the Single Cell 3′ Kit v3.1 (10X Genomics) according to the manufacturer's protocol. Sample quality was controlled with a Bioanalyzer Agilent 2100 using a High Sensitivity DNA chip (Agilent Genomics). Libraries were sequenced using an Illumina HiSeq 4000 to achieve a minimum depth of 100,000 raw reads per cell.

Lentiviral barcoding

The barcoded GFP-BC32 lentiviral-vector library was kindly provided by K. Cornils (University Medical Center, Hamburg, Germany).[51] UCB $CD34^+$ ($CD45RA^-CD38^-Lin^-$) cells (purity >90%) were exposed 6-h to the barcoded lentiviruses used at a multiplicity of infection allowing approximately 30% of transduction efficiency to ensure that that each cell contains only one integrated barcode. Infections were performed in RPMI medium supplemented with 20% BIT 9500 (StemCell Technologies) and SCF (50 ng/mL), FLT3L (50 ng/mL), TPO (20 ng/mL) and IL-3 (10 ng/mL; all from Miltenyi). NSG mice reconstituted with the lentivirally-transduced $CD34^+$ cells were sacrificed at week-3 after grafting before harvesting of BM and sorting of hu-$CD45^+$ cellular subsets, as above. To investigate the barcode content, the BC32 sequences were subjected to two rounds of amplification with common (DUAL_P5_01) or population-specific (MLPX35-42) primers. Barcode libraries were then pooled and sequenced with Illumina HiSeq 4000. Barcode analyses were performed as described with the genBaRcode package (https://cran.r-project.org/web/packages/genBaRcode).[52]

QUANTIFICATION AND STATISTICAL ANALYSIS

Mini-RNA-seq analysis

Data quality control and preprocessing

Data quality control and pre-processing were performed by SciLicium (Rennes, France). Briefly, the first read contains 16 bases that must have a quality score higher than 10. The first 6 bp correspond to a unique sample-specific barcode and the following 10 bp to a unique molecular identifier (UMI). The second reads were aligned to the human GRCh38/hg38 reference genome from the UCSC website using BWA version 0.7.4.4 with the parameter "–l 24". Reads mapping to several positions in the genome were filtered out from the analysis. The complete pipeline has been previously described in.[53] After quality control and data pre-processing, a gene count matrix was generated by counting the number of unique UMIs associated with each gene (lines) for each sample (columns). The UMI matrix was further normalized with the regularized log (rlog) transformation package implemented in the DeSeq2 package.[54]

Statistical filtration and clustering analysis

The statistical comparisons were performed in the AMEN suite of tools.[55] For each analysis relevant comparisons were selected to identify differentially expressed genes (DEGs). Briefly, genes showing an expression signal higher than 0.0 and at least a 2.0-fold-change between the two experimental conditions of each pairwise comparison were selected. The empirical Bayes moderated t-statistics implemented into the LIMMA package (F-value adjusted using the Benjamini & Hochberg (BH) False Discovery Rate approach, $p \leq 0.05$)[56–59] was used to define the set of genes showing significant statistical changes across all comparisons of a given transcriptomic analysis. The resulting set of DEGs were then partitioned into distinct expression clusters with the k-means algorithm and presented as heatmaps by using the pheatmap R package developed by R. Kolde (2019) (version 1.0.12. https://CRAN.R-project.org/package=pheatmap).

Single cell-RNA-seq analysis

Data quality control and preprocessing

Demultiplexed raw sequencing reads were processed, mapped to the GRCh38 human reference genome and quantified based on unique molecular identifiers (UMIs) with the Cell Ranger pipeline (v3.0.2, 10x Genomics). The resulting raw count matrices were then merged. Subsequently, the Scater R package (v1.10.1) was used to remove outlier cells by using several cell features including the proportions of reads mapping mitochondrial and ribosomal genes. In parallel, doublets were filtered out independently in each individual matrix by using the DoubletFinder R package (v.2.0.2). Cells with less than 1000 detected genes and genes detected in less than 10 cells were removed. Cells from all datasets were assigned a cell cycle phase by using Seurat. Data were normalized using the NormalizeData and the SCTransform functions implemented into Seurat.

Reduction of dimensionality and clustering

The top-3000 most varying genes were used to perform a principal component analysis with the RunPCA function implemented in Seurat. Cells were then clustered by using the FindNeighbors and FindClusters functions on the top-30 principal components, with default parameters. Finally, we used the uniform manifold approximation and projection (UMAP) method implemented in Seurat to project single cells in a reduced 2D space.

Cluster annotation and gene expression analysis

Cell clusters were annotated using a set of 42 known marker genes which are also significantly differentially expressed between cell clusters. Differentially expressed genes were identified with the FindAllMarkers function implemented in Seurat, with default parameters.

Trajectory inference and pseudotime analysis

Cell trajectories were inferred the getLineages followed by the getCurves functions implemented into the SlingShot package[41] on the scRNA-seq data by indicating the C1 cell cluster (HSC) as starting cells. Trajectory-based differential expression analysis was performed with the tradeSeq package by using the pseudotime values inferred by SlingShot for each lineage.[41,60]